

## Synthesis and in Vitro and in Vivo Evaluation of $^{18}\text{F}$ -Labeled Positron Emission Tomography (PET) Ligands for Imaging the Vesicular Acetylcholine Transporter

Zhude Tu,<sup>\*,†</sup> Simon M. N. Efange,<sup>‡</sup> Jinbin Xu,<sup>†</sup> Shihong Li,<sup>†</sup> Lynne A. Jones,<sup>†</sup> Stanley M. Parsons,<sup>§</sup> and Robert H. Mach<sup>†</sup>

Division of Radiological Sciences, Washington University School of Medicine, 510 South Kingshighway Boulevard, St. Louis, Missouri 63110, Department of Radiology, University of Minnesota, Minneapolis, Minnesota 55455, and Department of Chemistry and Biochemistry, University of California, Santa Barbara, California 93106

Received September 29, 2008

A new class of vesicular acetylcholine transporter inhibitor that incorporates a carbonyl group into the benzovesamicol structure was synthesized, and analogues were evaluated in vitro. ( $\pm$ )-*trans*-2-Hydroxy-3-(4-(4-[ $^{18}\text{F}$ ]fluorobenzoyl)piperidino)tetralin (**9e**) has  $K_i$  values of 2.70 nM for VACHT, 191 nM for  $\sigma_1$ , and 251 nM for  $\sigma_2$ . The racemic precursor (**9d**) was resolved via chiral HPLC, and ( $\pm$ )-[ $^{18}\text{F}$ ]**9e**, (-)-[ $^{18}\text{F}$ ]**9e**, and (+)-[ $^{18}\text{F}$ ]**9e** were respectively radiolabeled via microwave irradiation of the appropriate precursors with [ $^{18}\text{F}$ ]/F<sup>-</sup> and Kryptofix/K<sub>2</sub>CO<sub>3</sub> in DMSO with radiochemical yields of ~50–60% and specific activities of >2000 mCi/ $\mu\text{mol}$ . (-)-[ $^{18}\text{F}$ ]**9e** uptake in rat brain was consistent with in vivo selectivity for the VACHT with an initial uptake of 0.911 %ID/g in rat striatum and a striatum/cerebellum ratio of 1.88 at 30 min postinjection (p.i.). MicroPET imaging of macaques demonstrated a 2.1 ratio of (-)-[ $^{18}\text{F}$ ]**9e** in putamen versus cerebellum at 2 h p.i. (-)-[ $^{18}\text{F}$ ]**9e** has potential to be a PET tracer for clinical imaging of the VACHT.

### Introduction

Neurodegenerative diseases such as Alzheimer's disease, Down's syndrome, Parkinson's disease, and schizophrenia are generally characterized by progressive diminution in cognitive function associated with the loss of cholinergic neurons and synapses in the brain. For Alzheimer's disease, the severity of cognitive dysfunction is correlated with loss of cholinergic synaptic elements in the cortex and subcortical brain areas.<sup>1–7</sup> For Down's syndrome, presynaptic cholinergic deficits also contribute to loss of cognitive function.<sup>8–11</sup> For Parkinson's disease, patients exhibit subtle but early cognitive disturbances that correlate with cholinergic deficits in cortical areas.<sup>12,13</sup> For schizophrenia, cognitive dysfunction occurs in the early phases of the disease and remains throughout its course.<sup>14</sup> Although these disorders are all characterized by cognitive deficits, clinical and preclinical evidence demonstrates that the cholinergic deficits are localized to different components of the cholinergic system<sup>15–18</sup> and cholinergic innervations.<sup>19,20</sup> To date, the use of drugs that inhibit acetylcholinesterase to increase the availability of acetylcholine (ACh<sup>e</sup>) in the central cholinergic system is a major therapeutic approach to treatment of the cognitive dysfunctions.<sup>12,13,21–28</sup> For example, tacrine, donepezil, rivastig-

mine, and galantamine are four of the most widely used acetylcholinesterase inhibitors.<sup>29–31</sup>

In the central nervous system, ACh is the primary signaling molecule of cholinergic neurons. The vesicular acetylcholine transporter (VACHT) is responsible for transporting newly synthesized ACh into synaptic vesicles.<sup>32–34</sup> VACHT has been cloned from 12 species that include *C. elegans*, *Torpedo*, rat, and human.<sup>34–39</sup> It is a reliable molecular marker of the cholinergic system. Prado and colleagues<sup>40</sup> reported a strong relationship between the levels of VACHT expression and ACh release in both the peripheral and central nervous systems. A marked reduction of VACHT expression can affect neurotransmission at the neuromuscular junction. Even a modest deficiency of VACHT is sufficient to interfere with release of ACh in the brain and to alter cognitive behavior in object and social recognition and memory function.<sup>40</sup> Changes in VACHT expression levels have also been implicated in drug addiction, including addiction to nicotine, ethanol, and neurostimulants such as cocaine and amphetamine and opiates.<sup>41,42</sup> VACHT level in the brain is affected with drug abuse in humans; the levels of VACHT are subject to both up- and down-regulation as part of compensatory processes that attempt to maintain homeostasis of neuronal cholinergic activity.<sup>41</sup> If PET tracers could measure VACHT levels in vivo, they could be used as a biomarker for studying changes in cholinergic function in living animal or human brains in response to therapy.

The lead compound for all radiotracer development in this field is the aminoalcohol derivative vesamicol [(–)-*trans*-2-(4-phenylpiperidinyl)cyclohexanol]. However, since (–)-[ $^3\text{H}$ ]vesamicol was found to have a high affinity for  $\sigma_1$  and  $\sigma_2$  receptors in addition to the VACHT and to have marginal selectivity for VACHT versus  $\sigma_1$  and  $\sigma_2$  receptors,<sup>43</sup> there has been a vigorous effort to develop more selective VACHT ligands. Examples of the more prominent compounds are shown in Figure 1.

The class of compounds receiving the most attention for in vivo imaging is the benzovesamicol analogues, which consist of five compounds: aminobenzovesamicol (ABV), 4-fluoromethylvesamicol (FMV), (–)-5-(*N*-methylamino)benzovesamicol (MABV), (2)-*N*-ethyl-*N*-fluoroacetamidobenzovesamicol (NEFA),

\* To whom correspondence should be addressed. Telephone: 314-362-8487. Fax: 314-262-8555. E-mail: tuz@mir.wustl.edu.

<sup>†</sup> Washington University School of Medicine.

<sup>‡</sup> University of Minnesota.

<sup>§</sup> University of California.

<sup>a</sup> Abbreviations: VACHT, vesicular acetylcholine transporter; ACh, acetylcholine; HPLC, high performance liquid chromatography; TLC, thin layer chromatography; %ID/g, percent injected dose per gram; p.i., postinjection; PET, positron emission tomography; SPECT, single photon emission computed tomography; MRI, magnetic resonance imaging; ABV, aminobenzovesamicol; FMV, 4-fluoromethylvesamicol; MABV, (–)-5-(*N*-methylamino)benzovesamicol; NEFA, (2)-*N*-ethyl-*N*-fluoroacetamidobenzovesamicol; FEOBV, (–)-5-fluoroethoxybenzovesamicol; FBOV, 4-fluorobenzyloxyvesamicol; MIBT, *m*-iodobenzyltrozamicol; FBT, *p*-fluorobenzytrozamicol; IBVM, (–)-5-iodobenzovesamicol; DTG, 1,3-ditolyguanidine; Kryptofix, 4,7,13,16,21,24-hexaoxa-1,10-diazabicyclo[8.8.8]hexacosane; DMSO, dimethyl sulfoxide; DMF, *N,N*-dimethylformamide; NBS, *N*-bromosuccinimide; ND, not determined.

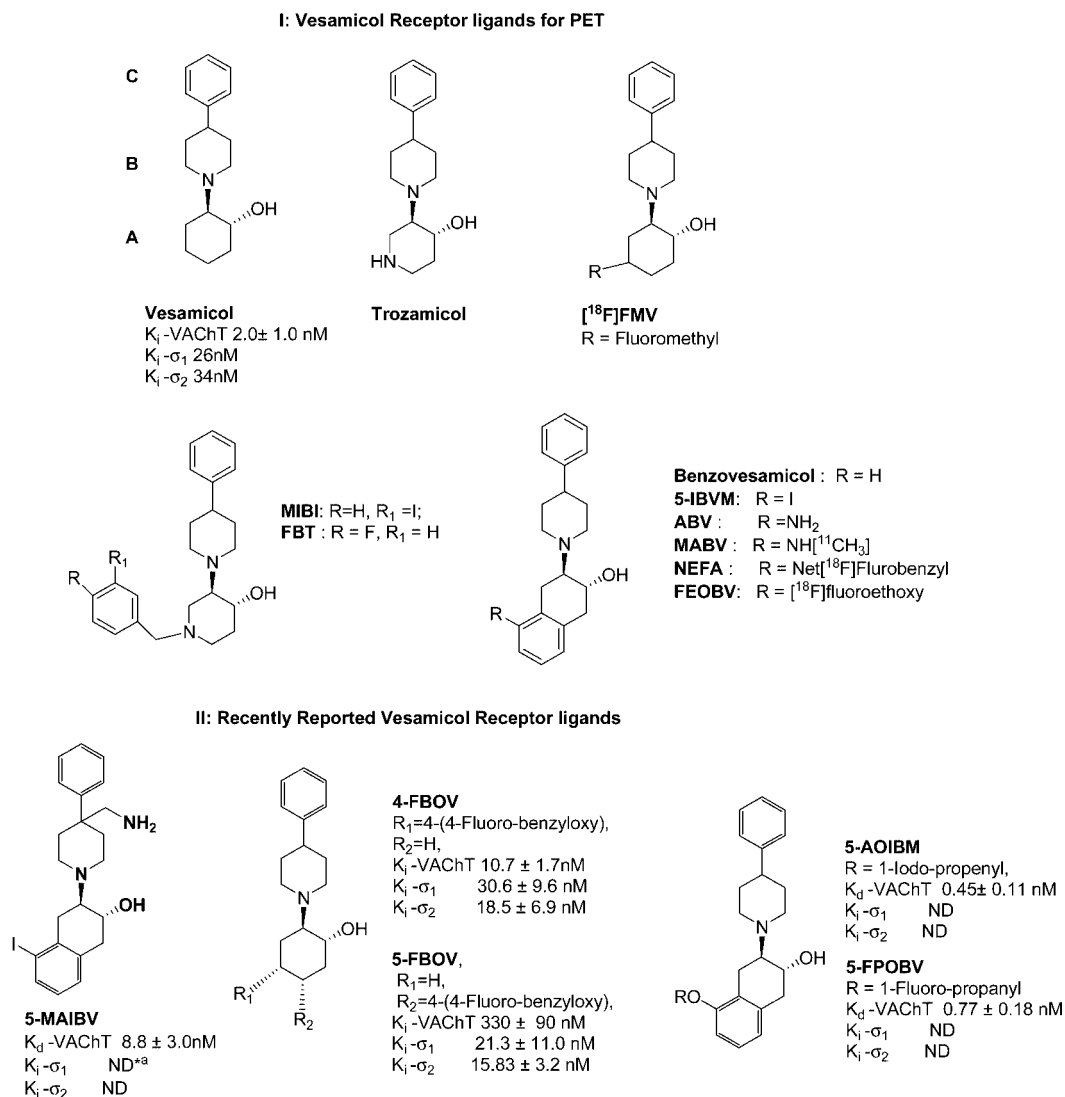


**Figure 1.** Structures and in vitro biological properties of ligands for the vesicular acetylcholine transporter: (\*a) ND, not determined. The new benzoylbenzovesamicol analogues interpose a carbonyl group between regions B and C.

and (–)-5-fluoroethoxybenzovesamicol (FEOBV) (Figure 1). Another analogue, (–)-5-iodobenzovesamicol (IBVM), has been radiolabeled with <sup>123</sup>I and used as a SPECT radiotracer to measure the cholinergic terminal density in human AD patients.<sup>44,45</sup> However, the high lipophilicity of [<sup>123</sup>I]IBVM, slow clearance from noncholinergic regions of brain, and irreversible kinetics from the regions with high density of cholinergic terminals in brain required that SPECT imaging studies be conducted 22 h following iv injection of the radiotracer. The long time interval required to achieve equilibrium is not compatible with the radioisotopes used in PET, particularly carbon-11 ( $t_{1/2} = 20.4$  min) and fluorine-18 ( $t_{1/2} = 109.8$  min). Recently, two 4-fluorobenzyloxy analogues of vesamicol, 4-(4-fluorobenzyloxy)vesamicol (4-FBOV) and 5-(4-fluorobenzyloxy)vesamicol (5-FBOV), were reported to have moderate or poor affinity for the VAcHT.<sup>46</sup> These compounds also displayed a high affinity for  $\sigma_1$  receptors (Figure 1). In addition, a number of benzovesamicol analogues displaying moderate to high affinity ( $K_d = 0.45$ – $8.8$  nM) for the VAcHT have been recently reported (Figure 1) as well as a series of methylvesamicol analogues.<sup>47,48</sup> It is not clear if these compounds will be useful for imaging the VAcHT with PET or SPECT.

Another class of compounds are the azavesamicol analogues represented by 4-[<sup>18</sup>F]-(+)-fluorobenzyltrozamicol ((+)-[<sup>18</sup>F]-

BT) and [<sup>125</sup>I]-*m*-iodobenzyltrozamicol ([<sup>125</sup>I]MIBT). The tracer (+)-[<sup>18</sup>F]FBT displayed good properties in animal imaging studies of rodents<sup>49</sup> and rhesus monkeys,<sup>50–52</sup> and has appropriate in vivo kinetics for PET studies of the VAcHT in anesthetized nonhuman primates with a low test–retest variability. However, (+)-[<sup>18</sup>F]FBT has a relatively high affinity for  $\sigma$  receptors, which resulted in unacceptably high nonspecific binding in human subjects (Mach unpublished data). Therefore, (+)-[<sup>18</sup>F]FBT is not clinically useful for imaging the VAcHT.

PET studies with VAcHT radiotracers have shown that most vesamicol analogues also display high affinity for  $\sigma$  receptors. This observation has been attributed to the high degree of structural similarity between pharmacophores for VAcHT and  $\sigma$  receptors. It has also been reported that in the rat brain,  $\sigma_1$  receptor density is highest in Purkinje cells of the cerebellum, the pons-medulla, midbrain, and hippocampus.<sup>56</sup> Moderate densities of  $\sigma$  receptor are found in the hypothalamus and cerebral cortex. Consequently, imaging data generated from a PET tracer for VAcHT that also labels  $\sigma$  receptors could lead to an inaccurate estimation of the amount of the VAcHT within these brain regions. Even though [<sup>123</sup>I]IBVM has been used as a SPECT imaging radiotracer to measure the VAcHT level in brain,<sup>45</sup> no PET radiotracers have been used in human imaging studies of the VAcHT. The higher sensitivity and quantitative

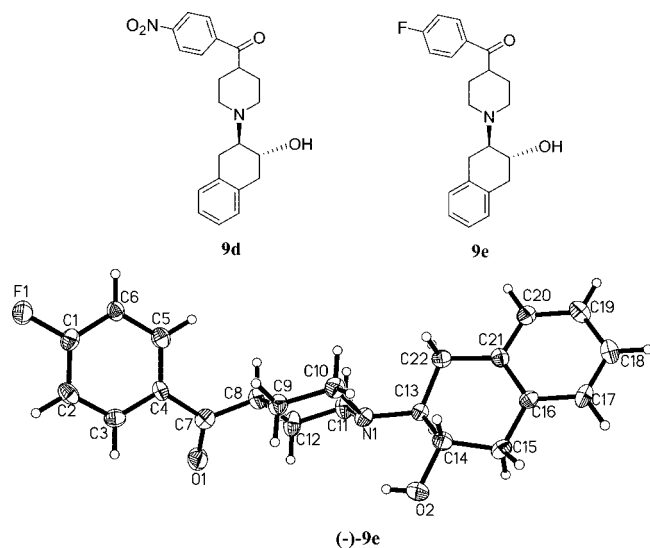


**Figure 2.** Chemical structures of **9d** and **9e** and the crystal structure of **(-)-9e**.

capability of PET versus SPECT indicate that there is a need to develop PET tracers for imaging the VACHT.

The structure of vesamicol, the prototypical VACHT ligand, may be divided into three identifiable regions of fragments labeled A, B, and C (Figure 1).<sup>43</sup> In this paper, we report the synthesis and in vitro characterization of a new class of vesamicol analogues that interpose a carbonyl group between regions B and C. We also described the optical resolution, radiolabeling, and in vitro and in vivo characterization of  $(\pm)$ -*trans*-2-hydroxy-3-(4-(4-[<sup>18</sup>F]fluorobenzoyl)piperidino)tetralin (**9e**), the most promising compound that emerged from this new group of vesamicol analogues. The crystal structure of **9e** is displayed in Figure 2.

Because the fluorine-containing analogue, **9e**, displayed high affinity for VACHT ( $K_i = 2.7$  nM) and good selectivity for the VACHT compared to  $\sigma_1$  and  $\sigma_2$  receptors ( $K_i = 191$  nM for  $\sigma_1$  and  $K_i = 251$  nM for  $\sigma_2$ ), the racemic mixture  $(\pm)$ -**9e** was resolved using chiral HPLC to obtain the pure enantiomers which were characterized in vitro. The minus isomer **(-)-9e** ( $K_i = 4.1$  nM) was more potent than the plus isomer **(+)-9e** ( $K_i = 108$  nM). In order to compare the enantiomers in vivo, the racemic precursor for radiolabeling (**9d**) was also resolved using chiral HPLC. The racemic mixture  $(\pm)$ -[<sup>18</sup>F]**9e**, plus isomer **(+)-[<sup>18</sup>F]9e**, and minus isomer **(-)-[<sup>18</sup>F]9e** were radiosynthesized successfully by microwave irradiation of the corresponding nitro substituted precursors with [<sup>18</sup>F]/fluoride and Kryptofix/K<sub>2</sub>CO<sub>3</sub> in DMSO and evaluated in male Sprague–Dawley rats to confirm that the distribution in the brain of **(-)-[<sup>18</sup>F]9e**, the most potent isomer, was consistent with the expression of the VACHT. **(-)-[<sup>18</sup>F]9e** was then evaluated in male rhesus monkeys to determine its potential as a PET radioligand for clinical imaging of the VACHT receptor.

## Results and Discussion

**Chemistry.** Vesamicol analogues are routinely synthesized by reacting a 4-substituted piperidine with an epoxide. Consequently, the synthesis of the target compounds began with the preparation of the corresponding 4-benzoylpiperidines **5a–d** (Scheme 1). Conversion of **1** into ethyl 1-benzoylpiperidine-4-carboxylate and then hydrolysis of the ester with sodium hydroxide gave the *N*-benzoyl protected isonipecotic acid **2** that provided a versatile intermediate for Friedel–Crafts acylation

to generate **3a** and **3b**. The bromophenyl analogue **3b** was treated with potassium phthalimide to give **4**, which was then hydrolyzed to generate the 4-amino intermediate **3c**. The 4-nitro compound, **3d** was obtained by oxidation of **3c** with *m*-chloroperoxybenzoic acid. Hydrolytic removal of the benzoyl group in **3a–d** generates the corresponding 4-benzoylpiperidine analogues **5a–d**. The fluorine-substituted analogue, 4-fluorobenzoylpiperidine **5e**, is commercially available.

Synthesis of **8** began with 1,4-dihydronaphthalene **6** as shown in Scheme 2. Compound **7** was generated by reacting **6** with *N*-bromosuccinimide. Then **8** was obtained by refluxing **7** in chloroform in the presence of aqueous sodium hydroxide. Reaction of **5a–e** with compound **8** in ethanol in the presence of Na<sub>2</sub>CO<sub>3</sub> afforded the corresponding products **9a–e** in moderate yields (Scheme 2). Compounds **9a–e** were converted into the corresponding hydrochloride salts for in vitro binding studies to determine the affinities for the VACHT and  $\sigma_1$  and  $\sigma_2$  receptors.

In vitro binding studies revealed that the racemic compound **9e** displayed a high affinity for the VACHT and moderate affinities for  $\sigma_1$  and  $\sigma_2$  receptors and was identified as a potential candidate for radiolabeling with <sup>18</sup>F. Compound **9e** was further resolved from the racemic mixture via chiral HPLC as described below to obtain the enantiomerically pure isomers.

Resolution of  $(\pm)$ -**9e** was performed by HPLC on a Chiralcel OD HPLC column, 250 mm × 10 mm, with a mobile phase of isopropanol/hexane (10:90) eluting at a flow rate of 5.0 mL/min. A UV wavelength of 254 nm was used for chiral resolution. Under these conditions, the retention time of **(+)-9e** is 14.38 min while the retention time of **(-)-9e** is 25.18 min.

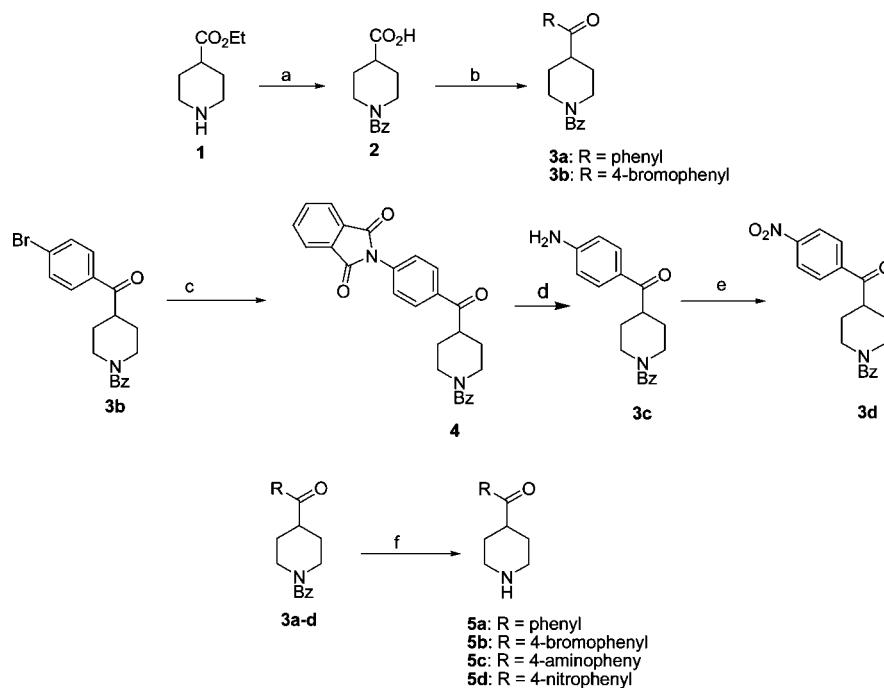
Compound **9d** serves as the precursor for radiosynthesis of [<sup>18</sup>F]**9e**. In order to prepare the pure enantiomers **(+)-[<sup>18</sup>F]9e** and **(-)-[<sup>18</sup>F]9e**, the corresponding enantiomerically pure isomers **(+)-9d** and **(-)-9d** were also obtained by performing HPLC on a Chiralcel OD HPLC column (250 mm × 10 mm) using isopropanol/hexane (18:82) at a flow rate of 5.0 mL/min. A UV wavelength of 254 nm was used for chiral resolution. Under these conditions the retention time of **(+)-9d** is 22.13 min while the retention time of **(-)-9d** is 38.13 min.

The crystal structure of **(-)-9e** was unequivocally determined by X-ray diffraction of the corresponding **(-)-9e** hydrochloride. The colorless crystals of **(-)-9e** were grown by slow evaporation of ethanol/methylene chloride solutions of the compound at 23 °C. The crystal structure of **(-)-9e** is presented in Figure 2.

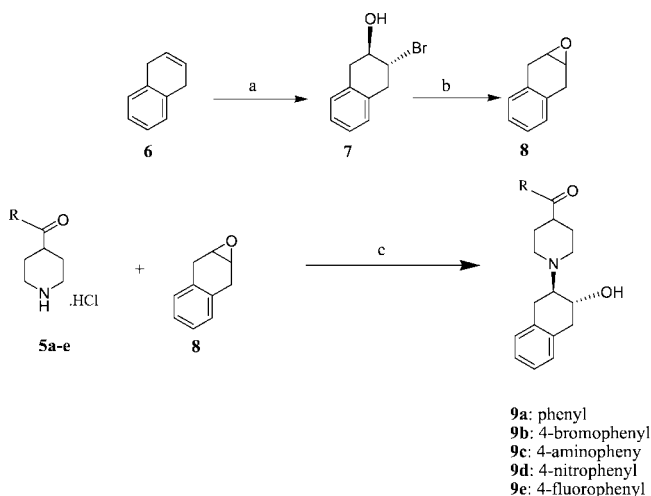
The radiosynthesis of **(+)-[<sup>18</sup>F]9e**, **(-)-[<sup>18</sup>F]9e**, and  $(\pm)$ -[<sup>18</sup>F]**9e** was accomplished by treating the corresponding precursors **(+)-9d**, **(-)-9d**, and  $(\pm)$ -**9d** with [<sup>18</sup>F]fluoride/K<sub>2</sub>CO<sub>3</sub> and Kryptofix in DMSO (Scheme 3). The reaction mixture was irradiated for 30–40 s in a microwave oven, and the crude product was separated from the unreacted [<sup>18</sup>F]fluoride by passing the mixture through a Sep-Pak light alumina N cartridge with 3.0 mL of mobile phase (THF/0.1 M ammonium formate buffer (23:77)). The crude product was then purified by HPLC on an Alltech Econosil C-18 reversed-phase column (250 mm × 10 mm). At 3.5 mL/min flow rate using the mobile phase described above, the retention time of the production is ~12.6 min. The entire procedure required ~2 h, and the radiochemical yield was 50–60% (decay-corrected to the start of synthesis). The specific activity was >2000 Ci/mmol.

**In Vitro Binding Studies.** In vitro binding studies were conducted to measure the affinities of the target compounds for the VACHT and for  $\sigma_1$  and  $\sigma_2$  receptors.

The binding assays used [<sup>3</sup>H]vesamicol for VACHT, **(+)-[<sup>3</sup>H]pentazocine** for the  $\sigma_1$  receptors, and [<sup>3</sup>H]DTG in the

Scheme 1<sup>a</sup>

<sup>a</sup> Reagents and conditions: (a) (i) benzoyl chloride, Et<sub>3</sub>N; (ii) NaOH, aq EtOH; (b) (i) oxalyl chloride, CH<sub>2</sub>Cl<sub>2</sub>; (ii) arene, AlCl<sub>3</sub>, CS<sub>2</sub>, reflux; (c) phthalimide-K, CuI, DMA, heat; (d) 32% HBr–HOAc, 45 °C; (e) *m*CPBA, CHCl<sub>3</sub>, heat; (f) 6 N HCl, heat.

Scheme 2<sup>a</sup>

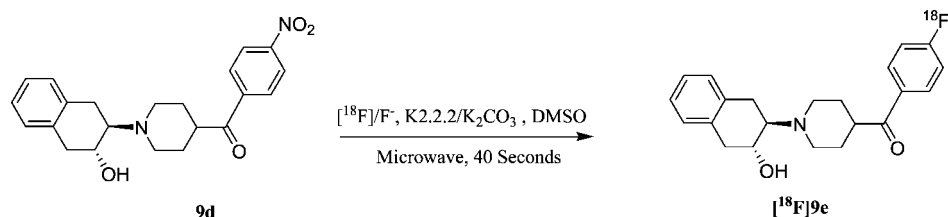
<sup>a</sup> Reagents and conditions: (a) NBS, aqueous THF; (b) aqueous NaOH, CHCl<sub>3</sub>, reflux; (c) EtOH, Et<sub>3</sub>N, reflux.

presence of 1  $\mu$ M (+)-pentazocine for the  $\sigma_2$  receptor. The  $K_i$  values were determined from competition plots. The results of the binding assays for compounds **9a–d**, ( $\pm$ )-**9e**, (+)-**9e**, (–)-**9e** are shown in Table 1. Substituting the 4-position of the phenyl group of **9a** with Br, NH<sub>2</sub>, NO<sub>2</sub>, or F generated **9b**, **9c**, **9d**, or **9e**. The affinities for VACHT are Br > NO<sub>2</sub> > NH<sub>2</sub> > F > H, corresponding to the following IC<sub>50</sub> values: 0.25  $\pm$  0.02, 0.48  $\pm$  0.03, 1.68  $\pm$  0.04, 2.70  $\pm$  0.40, 4.30  $\pm$  1.00 nM. The bromine compound **9b** has the highest affinity for the VACHT. The fluorine substituted compound **9e** also has a moderate affinity of 2.70  $\pm$  0.40 nM, which is comparable to the  $K_i$  value of vesamicol. The bromine and fluorine substituted compounds **9b** and **9e** are potential PET radiotracers when labeled respectively with <sup>76</sup>Br and <sup>18</sup>F. Three of the five benzoylpiperidine-containing compounds, **9a**, **9b**, and **9e**, displayed significantly lower affinity for VACHT than (+)-FBT (Table 1). For the two halogenated

analogues, **9b** and **9e**, affinities of  $\sigma_1$  and  $\sigma_2$  receptors were at least 10-fold lower than those reported for (+)-FBT. In terms of VACHT/ $\sigma$  selectivity, the bromine analogue **9b** was superior to the fluorine compound **9e**, with a calculated selectivity ratio of 297 versus 71.

By comparison of the two halogenated compounds, it was observed that the bromine analogue **9b** displays higher affinity for VACHT than the fluorine compound **9e**. Additionally, **9b** exhibits lower affinity for both  $\sigma_1$  and  $\sigma_2$  receptors than **9e**. As a result, the bromine compound displays considerably higher VACHT/ $\sigma$  selectivity than **9e**. Both compounds are moderately lipophilic, as revealed by their calculated log *P* values (Table 1); consequently, they are expected to cross the blood–brain barrier. However, the radionuclidic properties of <sup>76</sup>Br make it less than ideal for PET imaging when compared with <sup>18</sup>F. Radiotracers containing <sup>18</sup>F give higher quality PET images than those containing <sup>76</sup>Br because of both the prompt  $\gamma$  emissions and the long positron range of <sup>76</sup>Br. Although correction factors have been proposed to remove the cascade coincidences, because positron range is a limiting factor for spatial resolution on PET scanners, radionuclides like <sup>76</sup>Br with a longer mean positron range (3.47 mm in water) than the mean positron range of <sup>18</sup>F (0.51 mm in water) create inherently “blurred” images.<sup>53–55</sup> Because of these considerations, we chose to initially radiolabel **9e** rather than **9b**. Optical resolution of ( $\pm$ )-**9e** and characterization of the enantiomers showed that the (–)-**9e** displayed improved VACHT/ $\sigma$  selectivity over the racemic mixture in vitro, thereby providing further support for radiolabeling the ligand for in vivo studies.

**In Vivo Rat Biodistribution Studies.** The results of the tissue biodistribution studies of (–)-[<sup>18</sup>F]**9e**, (+)-[<sup>18</sup>F]**9e**, and ( $\pm$ )-[<sup>18</sup>F]**9e** in adult male Sprague–Dawley rats are reported as percent injected dose per gram (%ID/g) and summarized in Table 2. The initial brain uptake values were 0.823, 0.350, 0.606 %ID/g for (–)-[<sup>18</sup>F]**9e**, (+)-[<sup>18</sup>F]**9e**, ( $\pm$ )-[<sup>18</sup>F]**9e**, respectively. At all time points postinjection (p.i.), the minus isomer (–)-[<sup>18</sup>F]**9e** displayed a higher brain uptake and lower initial blood

Scheme 3. Radiosynthesis of (±)-[<sup>18</sup>F]9e, (+)-[<sup>18</sup>F]9e, and (-)-[<sup>18</sup>F]9Table 1. Affinities ( $K_i$ ) of the Benzoylbenzovesamicol Analogues **9a–e**, (+)-**9e**, (-)-**9e** for VACHT and  $\sigma_1$  and  $\sigma_2$  Receptors Assayed in Vitro<sup>a</sup>

ligands	$K_i$ (nM)			VACHT/ $\sigma$ ratio		log $P^c$
	VACHT <sup>b</sup>	$\sigma_1^c$	$\sigma_2^d$	VACHT/ $\sigma_1$	VACHT/ $\sigma_2$	
vesamicol <sup>f</sup>	2.0 ± 1.0	25.8 ± 8.0	34.5 ± 2.0	25.8	34.5	1.40
benzovesamicol <sup>g</sup>	0.055 ± 0.01	ND	ND	ND	ND	2.44
(+)-FBT <sup>h</sup>	0.22 ± 0.05	21.6 ± 3.9	35.9 ± 6.3	98	163	1.99
<b>9a</b>	4.30 ± 1.00	219.6 ± 17.3	320.0 ± 6.6	51	74	2.78
<b>9b</b>	0.25 ± 0.02	297.7 ± 18.7	592.6 ± 95.2	1188	2368	3.73
<b>9c</b>	1.68 ± 0.14	ND	ND	ND	ND	1.56
<b>9d</b>	0.48 ± 0.03	ND	ND	ND	ND	2.16
(±)- <b>9e</b>	2.70 ± 0.40	191.1 ± 57.7	251.3 ± 39.2	71	93	2.99
(+)- <b>9e</b>	108 ± 15	185.97 ± 38.89	277.93 ± 26.66	1.7	2.8	2.99
(-)- <b>9e</b>	4.1 ± 0.6	658.60 ± 118.40	319.23 ± 36.64	160	78	2.99

<sup>a</sup>  $K_i$  values (mean ± SEM) were determined from at least three experiments. <sup>b</sup>  $K_i$  VACHT is measured using Torpedo synaptic vesicles. <sup>c</sup>  $\sigma_1$  binding is measured using guinea pig brain membranes. <sup>d</sup>  $\sigma_2$  binding is measured using rat liver preparations. <sup>e</sup> Calculated value at pH 7.4 by ACD/I-Lab, version 7.0 (Advanced Chemistry Development, Inc., Canada). <sup>f</sup> Reference 43. <sup>g</sup> Reference 62. <sup>h</sup> Reference 51.

Table 2. Biodistribution of (-)-[<sup>18</sup>F]9e, (+)-[<sup>18</sup>F]9e, and (±)-[<sup>18</sup>F]9e in Male Sprague Dawley Rats<sup>a</sup>

	compd	%ID/g			
		5 min	30 min	1 h	2 h
blood	(-)-[ <sup>18</sup> F]9e	0.073 ± 0.010	0.037 ± 0.002	0.029 ± 0.005	0.020 ± 0.002
	(+)-[ <sup>18</sup> F]9e	0.136 ± 0.020	0.087 ± 0.016	0.048 ± 0.007	0.027 ± 0.002
	(±)-[ <sup>18</sup> F]9e	0.122 ± 0.023	0.071 ± 0.009	0.043 ± 0.003	0.027 ± 0.004
lung	(-)-[ <sup>18</sup> F]9e	1.577 ± 0.224	0.481 ± 0.088	0.327 ± 0.022	0.199 ± 0.032
	(+)-[ <sup>18</sup> F]9e	0.904 ± 0.161	0.332 ± 0.073	0.188 ± 0.035	0.112 ± 0.023
	(±)-[ <sup>18</sup> F]9e	1.389 ± 0.247	0.553 ± 0.056	0.346 ± 0.045	0.223 ± 0.014
heart	(-)-[ <sup>18</sup> F]9e	0.321 ± 0.027	0.109 ± 0.014	0.066 ± 0.008	0.047 ± 0.009
	(+)-[ <sup>18</sup> F]9e	0.194 ± 0.006	0.094 ± 0.013	0.051 ± 0.005	0.031 ± 0.006
	(±)-[ <sup>18</sup> F]9e	0.328 ± 0.014	0.141 ± 0.005	0.094 ± 0.008	0.056 ± 0.007
muscle	(-)-[ <sup>18</sup> F]9e	0.091 ± 0.018	0.080 ± 0.008	0.056 ± 0.010	0.035 ± 0.007
	(+)-[ <sup>18</sup> F]9e	0.047 ± 0.010	0.051 ± 0.010	0.034 ± 0.008	0.022 ± 0.005
	(±)-[ <sup>18</sup> F]9e	0.079 ± 0.015	0.071 ± 0.006	0.076 ± 0.012	0.047 ± 0.006
fat	(-)-[ <sup>18</sup> F]9e	0.132 ± 0.095	0.207 ± 0.018	0.241 ± 0.021	0.249 ± 0.036
	(+)-[ <sup>18</sup> F]9e	0.052 ± 0.017	0.108 ± 0.053	0.154 ± 0.065	0.150 ± 0.062
	(±)-[ <sup>18</sup> F]9e	0.088 ± 0.026	0.177 ± 0.039	0.196 ± 0.035	0.173 ± 0.042
liver	(-)-[ <sup>18</sup> F]9e	1.506 ± 0.186	1.769 ± 0.179	2.214 ± 0.323	1.791 ± 0.297
	(+)-[ <sup>18</sup> F]9e	1.849 ± 0.566	1.239 ± 0.271	0.814 ± 0.120	0.692 ± 0.081
	(±)-[ <sup>18</sup> F]9e	1.939 ± 0.382	1.504 ± 0.271	1.402 ± 0.102	1.188 ± 0.158
kidney	(-)-[ <sup>18</sup> F]9e	2.018 ± 0.448	1.896 ± 0.333	1.298 ± 0.372	1.339 ± 0.160
	(+)-[ <sup>18</sup> F]9e	0.791 ± 0.123	0.416 ± 0.048	0.291 ± 0.032	0.194 ± 0.027
	(±)-[ <sup>18</sup> F]9e	1.644 ± 0.232	1.042 ± 0.205	0.990 ± 0.321	0.853 ± 0.171
bone	(-)-[ <sup>18</sup> F]9e	0.334 ± 0.047	0.157 ± 0.004	0.148 ± 0.015	0.138 ± 0.006
	(+)-[ <sup>18</sup> F]9e	0.187 ± 0.015	0.277 ± 0.080	0.399 ± 0.078	0.532 ± 0.096
	(±)-[ <sup>18</sup> F]9e	0.307 ± 0.011	0.445 ± 0.032	0.623 ± 0.080	0.739 ± 0.044
brain	(-)-[ <sup>18</sup> F]9e	0.823 ± 0.091	0.226 ± 0.014	0.124 ± 0.013	0.095 ± 0.016
	(+)-[ <sup>18</sup> F]9e	0.350 ± 0.040	0.071 ± 0.012	0.041 ± 0.002	0.022 ± 0.004
	(±)-[ <sup>18</sup> F]9e	0.606 ± 0.100	0.153 ± 0.044	0.095 ± 0.012	0.059 ± 0.008

<sup>a</sup> %ID/g values (mean ± SD) with  $n = 4$  rats per group.

uptake than the plus isomer (+)-[<sup>18</sup>F]9e. Modest but progressive accumulation of radioactivity was observed in bone tissue for racemic (±)-[<sup>18</sup>F]9e and (+)-[<sup>18</sup>F]9e in rats. The progressive increase in bone uptake was most likely the result of defluorination. For (+)-[<sup>18</sup>F]9e, bone uptake increased from 0.187 %ID/g at 5 min to 0.532 %ID/g at 2 h p.i. At the same time, bone uptake following injection of racemic (±)-[<sup>18</sup>F]9e increased from 0.31 %ID/g at 5 min to 0.739 %ID/g at 2 h p.i. In contrast, (-)-[<sup>18</sup>F]9e washed out of the bone between 5 min and 2 h p.i. (bone uptake was 0.334 %ID/g at 5 min and 0.138 %ID/g at 2 h) and thus does not appear to undergo defluorination in vivo.

For (-)-[<sup>18</sup>F]9e, the initial uptake of the blood was low and the clearance of this radiotracer from the blood was quite rapid,

yielding %ID/g values of 0.077, 0.037, 0.029, 0.020 at 5 min, 30 min, 1 h, and 2 h p.i., respectively. Apart from the lung, liver, and kidney, where the initial tracer uptakes 5 min p.i. were 1.58, 1.51, and 2.02 %ID/g, respectively, all other tissues displayed initial uptake values below 1.0 %ID/g.

Following injection of (-)-[<sup>18</sup>F]9e, radioactivity in the brain reached a level of 0.823 %ID/g at 5 min p.i.; thereafter, the level declined to 0.226, 0.124, and 0.095 %ID/g at 30 min, 1 h, and 2 h p.i., respectively. In contrast, the levels of radioactivity obtained in the brain following injection of (+)-[<sup>18</sup>F]9e were 0.350, 0.071, 0.041, 0.022 %ID/g at 5 min, 30 min, 1 h, and 2 h, respectively. Therefore, both the initial accumulation and subsequent retention are greater for (-)-[<sup>18</sup>F]9e than for (+)-

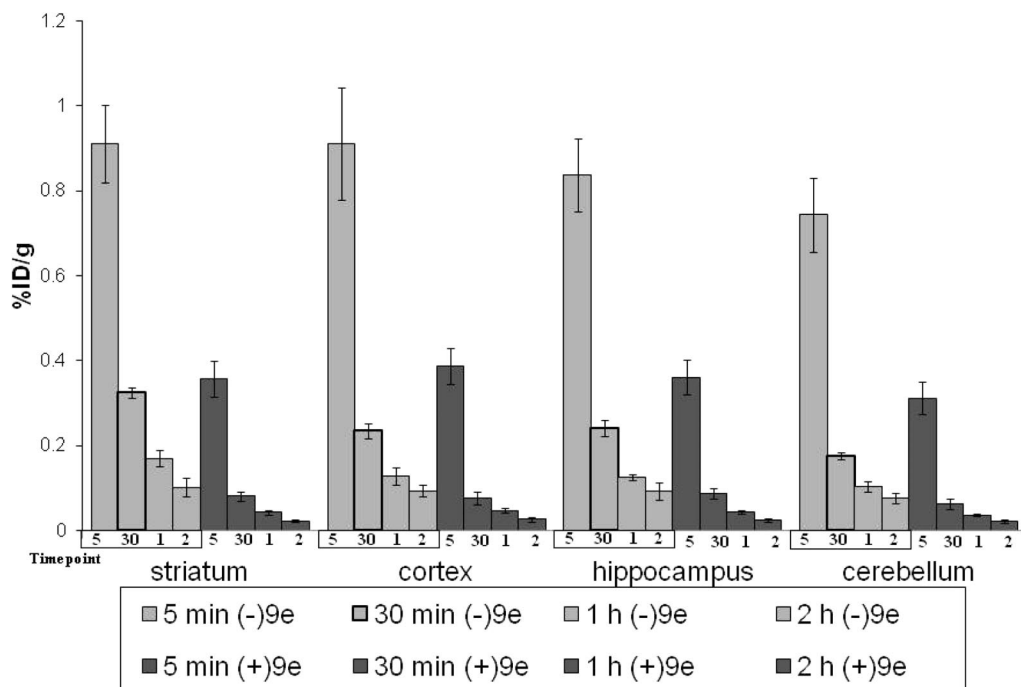


**Figure 3.** Regional brain uptake of (-)-[ $^{18}\text{F}$ ]9e and (+)-[ $^{18}\text{F}$ ]9e in male Sprague–Dawley rats from 5 min to 2 h p.i. The active enantiomer, (-)-[ $^{18}\text{F}$ ]9e, has higher striatal uptake at all time points.

**Table 3.** Ratio<sup>a</sup> of Striatum/Nonstriatal Tissue for (-)-[ $^{18}\text{F}$ ]9e and (+)-[ $^{18}\text{F}$ ]9e in Male Sprague–Dawley Rats

	compd	5 min	30 min	1 h	2 h
striatum/blood	(-)-[ $^{18}\text{F}$ ]9e	12.55 ± 0.77	8.86 ± 0.29	5.97 ± 1.12	5.17 ± 0.73
	(+)-[ $^{18}\text{F}$ ]9e	2.67 ± 0.57	0.95 ± 0.18	0.9 ± 0.23	0.87 ± 0.11
striatum/cortex	(-)-[ $^{18}\text{F}$ ]9e	1.00 ± 0.05	1.39 ± 0.05	1.36 ± 0.23	1.09 ± 0.15
	(+)-[ $^{18}\text{F}$ ]9e	0.92 ± 0.02	1.08 ± 0.09	0.95 ± 0.09	0.91 ± 0.15
striatum/hippocampus	(-)-[ $^{18}\text{F}$ ]9e	1.09 ± 0.01	1.36 ± 0.12	1.35 ± 0.11	1.11 ± 0.18
	(+)-[ $^{18}\text{F}$ ]9e	0.99 ± 0.04	0.93 ± 0.03	0.98 ± 0.14	0.99 ± 0.08
striatum/cerebellum	(-)-[ $^{18}\text{F}$ ]9e	1.23 ± 0.11	1.85 ± 0.06	1.64 ± 0.18	1.32 ± 0.07
	(+)-[ $^{18}\text{F}$ ]9e	1.15 ± 0.04	1.3 ± 0.07	1.17 ± 0.12	1.14 ± 0.09
striatum/total brain	(-)-[ $^{18}\text{F}$ ]9e	1.11 ± 0.04	1.44 ± 0.07	1.38 ± 0.13	1.08 ± 0.10
	(+)-[ $^{18}\text{F}$ ]9e	1.02 ± 0.03	1.13 ± 0.04	1.02 ± 0.09	1.04 ± 0.06

<sup>a</sup> Calculated from %ID/g striatum divided by %ID/g nonstriatal tissue with  $n = 4$  rats per group.

[ $^{18}\text{F}$ ]9e. The regional distribution of (-)-[ $^{18}\text{F}$ ]9e within the brain also suggests that it is selectively retained in regions (i.e., striatum) with a high VACHT density while (+)-[ $^{18}\text{F}$ ]9e displayed a relatively homogeneous uptake (Figure 3), consistent with the enantioselectivity observed previously with other benzovesamicol analogues and in our own in vitro studies (Table 1).

Brain dissection studies revealed that (-)-[ $^{18}\text{F}$ ]9e uptake was high in the striatum, moderate in the cortex and hippocampus, and low in the cerebellum. Initial brain uptake of (-)-[ $^{18}\text{F}$ ]9e at 5 min p.i. was relatively homogeneous with 0.911 %ID/g for striatum, 0.911 %ID/g for cortex, 0.837 %ID/g for hippocampus, and 0.743 %ID/g for cerebellum (Figure 3). However, the differences in regional tracer uptake became more pronounced over time, resulting in striatum/blood, striatum/cortex, striatum/hippocampus, striatum/cerebellum, and striatum/total brain ratios of 8.86, 1.39, 1.36, 1.88, and 1.44, respectively, at 30 min following tracer injection (Table 3). Therefore, the regional distribution of (-)-[ $^{18}\text{F}$ ]9e in the brain also mirrors VACHT density in this organ.<sup>56–58</sup>

**Ex Vivo Autoradiography of Rat Brain.** In order to confirm the striatal uptake of (-)-[ $^{18}\text{F}$ ]9e in rat brain, (-)-[ $^{18}\text{F}$ ]9e was injected iv into a male Sprague–Dawley rat, which was sacrificed 1 h p.i., and the brain was quickly removed and sliced into 1 mm coronal sections for digital autoradiography. Exami-

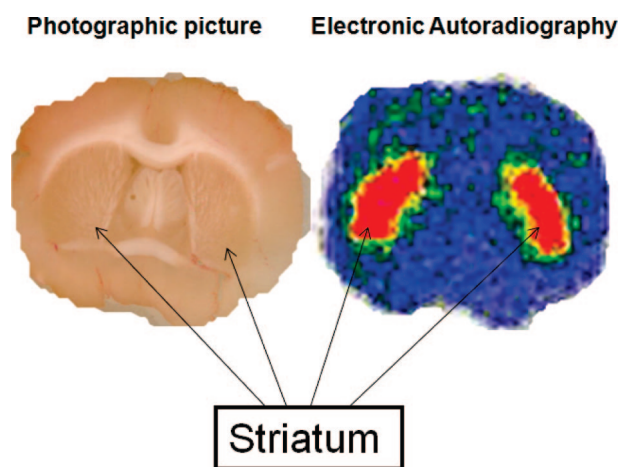


**Figure 4.** Ex vivo electronic autoradiography on a 1.0 mm slice through the striatum. The rat was sacrificed 60 min p.i. with 500  $\mu\text{Ci}$  (-)-[ $^{18}\text{F}$ ]9e. The left is the photographic picture of the slice acquired on a flatbed scanner. The right is the electronic autoradiography picture. These data demonstrate striatal localization of (-)-[ $^{18}\text{F}$ ]9e in Sprague–Dawley rats.

nation of the autoradiogram (Figure 4) reveals that (-)-[ $^{18}\text{F}$ ]9e has a high accumulation in the striatum and moderate accumulation in the cortex, a finding that is consistent with the data

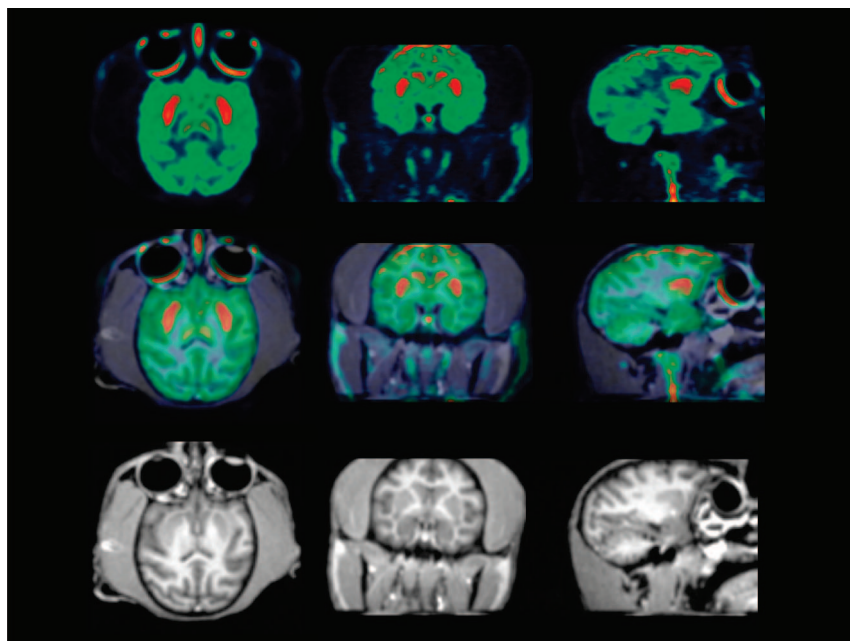


**Figure 5.** Representative microPET (top), MRI (bottom), and coregistered images (middle). PET images are summed images (0–120 min) over a 2 h dynamic scan, obtained by injection of (–)-[<sup>18</sup>F]9e into a rhesus monkey. High uptake of (–)-[<sup>18</sup>F]9e is observed in the putamen and caudate.

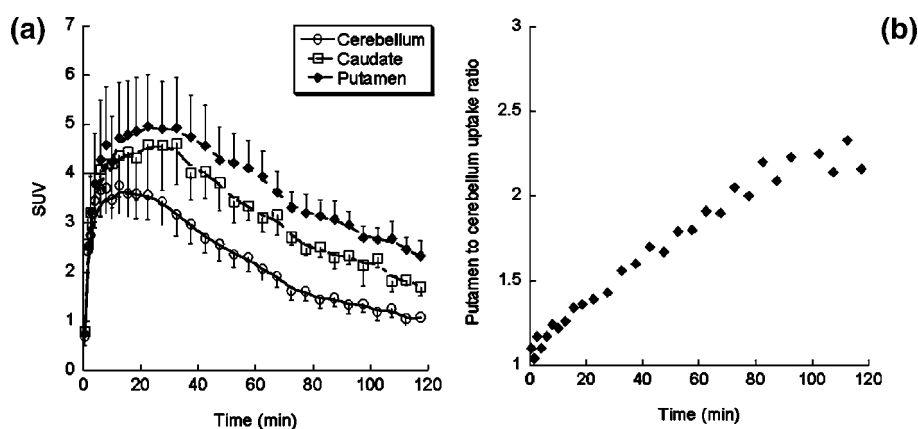


**Figure 6.** (A) Tissue time–activity curves of (–)-[<sup>18</sup>F]9e in the monkey brain. Each point shows the SUV mean  $\pm$  SEM of three monkeys. The uptake of (–)-[<sup>18</sup>F]9e in the brain reaches peak accumulation in the caudate and putamen at 30 min p.i. (B) Average striatum to cerebellum ratio of (–)-[<sup>18</sup>F]9e in three monkey brains. The ratio of striatum to cerebellum displays increasing activity in the striatum over time. At 2 h p.i., the striatum to cerebellum ratio reaches 2.1- to 2.3-fold.

obtained from tissue dissection studies in the rat and the known relative density of VACHT in the brain.

**MicroPET Imaging Study of Rhesus Monkeys.** The results of the rodent brain distribution studies and ex vivo autoradiographic studies suggest that (–)-[<sup>18</sup>F]9e may be a suitable ligand for studying cholinergic innervations via the VACHT in humans. To confirm the feasibility of using (–)-[<sup>18</sup>F]9e for measuring the density of VACHT in vivo, PET imaging studies with (–)-[<sup>18</sup>F]9e were conducted in three male rhesus monkeys (Figures 5 and 6) on a microPET Focus 220 scanner (Concorde/CTI/Siemens Microsystems, Knoxville, TN). A representative summed image from a microPET study of a male rhesus macaque injected with (–)-[<sup>18</sup>F]9e demonstrated high uptake of (–)-[<sup>18</sup>F]9e in the caudate and putamen (Figure 5, upper), which is a region expressing a high density of the VACHT. These data indicate that (a) (–)-[<sup>18</sup>F]9e enters the brain readily and (b) the distribution of (–)-[<sup>18</sup>F]9e is consistent with the distribution of the VACHT in brain. The tissue time–activity curves (Figure 6A) indicate that peak uptake of (–)-[<sup>18</sup>F]9e in caudate and

putamen occurred at about 30 min post-iv injection. Figure 6B indicates that the putamen/cerebellum ratio increases with time, reaching a value of 2.1 at 2 h. These data indicate that (–)-[<sup>18</sup>F]9e is a promising and novel PET radiotracer for imaging the VACHT. Further studies will be required to determine if (–)-[<sup>18</sup>F]9e can be used in clinical imaging studies.

## Conclusion

In the present study, we synthesized a new class of compounds targeting the VACHT by replacing the phenyl group in benzovesamicol with a substituted benzoyl moiety. In vitro binding assays of this new class of compounds suggested that this modification of vesamicol yields analogues with not only an increased affinity for VACHT but also high selectivity for VACHT versus  $\sigma$  receptors. For example, compound 9b has very high affinity for VACHT ( $K_i = 0.25 \pm 0.02$  nM) and very low affinity for  $\sigma$  receptors ( $K_i = 297.7 \pm 18.7$  nM for  $\sigma_1$ ,  $K_i = 592.6 \pm 95.2$  nM for  $\sigma_2$ ). In vivo evaluation of (±)-[<sup>18</sup>F]9d, (+)-[<sup>18</sup>F]9e, and (–)-[<sup>18</sup>F]9e demonstrated that (–)-[<sup>18</sup>F]9e not

only is more potent than (+)-[<sup>18</sup>F]9e but is also retained in target regions of the brain. The synthesis and radiosynthesis are straightforward: (–)-[<sup>18</sup>F]9e was easily produced with good yield and high specific activity in a simple one-step reaction. More importantly, (–)-[<sup>18</sup>F]9e not only demonstrated a high initial uptake (0.911 %ID/g for striatum at 5 min p.i.) and high target to nontarget ratio (1.88-fold at 30 min) in rat brain but also displayed a clear image of striatal tissue in rhesus monkey brain. In conclusion, the initial studies suggest that (–)-[<sup>18</sup>F]9e has excellent potential to be a novel PET tracer for clinical imaging studies of the VACHT.

## Experimental Section

**Materials.** All reagents and chemicals were purchased from commercial suppliers and used without further purification unless otherwise stated. Tetrahydrofuran (THF) was distilled from sodium hydride immediately prior to use. Anhydrous toluene was distilled from sodium/toluene shortly before use.

**General.** All anhydrous reactions were carried out in oven-dried glassware under an inert nitrogen atmosphere unless otherwise stated. When the reactions involved extraction with methylene chloride (CH<sub>2</sub>Cl<sub>2</sub>), chloroform (CHCl<sub>3</sub>), ethyl acetate (EtOAc), or ethyl ether (Et<sub>2</sub>O), the organic solutions were dried with anhydrous Na<sub>2</sub>SO<sub>4</sub> and concentrated with a rotary evaporator under reduced pressure. Flash column chromatography was conducted using silica gel 60A, “40 Micron Flash” [32–63 μm] (Scientific Adsorbents, Inc.); the mobile phase used is reported in the experimental procedure for each compound. Melting points were determined using the MEL-TEMP 3.0 apparatus and left uncorrected. <sup>1</sup>H NMR spectra were recorded at 300 MHz on a Varian Mercury-VX spectrometer with CDCl<sub>3</sub> as solvent and tetramethylsilane (TMS) as the internal standard. All chemical shift values are reported in parts per million (ppm) (δ). The mass spectra were recorded on a JKS-HX 11UHF/HX110 HF tandem mass spectrometer in the fast atom bombardment (FAB+) mode. Elemental analyses (C, H, N) were determined by Atlantic Microlab, Inc.

[<sup>18</sup>F]Fluoride was produced in our institution by <sup>18</sup>O(p, n)<sup>18</sup>F reaction through proton irradiation of enriched <sup>18</sup>O water (95%) using a JSW BC-16/8 (Japan Steel Works), CS-15 cyclotron (Cyclotron Corp., Berkeley, CA), or a RDS111 cyclotron (Siemens/CTI Molecular Imaging, Knoxville, TN). [<sup>18</sup>F]Fluoride is first passed through an ion-exchange resin and then is extracted with 0.02 M potassium carbonate (K<sub>2</sub>CO<sub>3</sub>) solution. The radiochemical and chemical purities were analyzed by reversed-phase C-18 HPLC with UV–visible and NaI detectors.

**1-Benzoylpiperidine-4-carboxylic Acid (2).** Benzoyl chloride (21.1 g, 150 mmol) was added dropwise with stirring to a solution of ethyl isonipicotate (1) (23.58 g, 150 mmol) and triethylamine (22.8 g, 225 mmol) in methylene chloride (250 mL). Following the addition, the reaction mixture was stirred overnight, then treated with water (30 mL) and stirred for an additional 10 min. The layers were separated, and the organic extract was washed consecutively with 0.6 M HCl and saturated sodium bicarbonate. After drying over anhydrous sodium sulfate, the solution was concentrated to yield 39 g of ester. <sup>1</sup>H NMR (CDCl<sub>3</sub>): δ 1.20–1.26 (t, 3H), 4.09–4.19 (q, 2H), 1.60–4.75 (m, 9H), 7.26–7.50 (m, 5H).

The ester was redissolved in 70% aqueous ethanol (150 mL). Then NaOH pellets (15 g, 375 mmol) were added into the above solution. The reaction mixture was stirred overnight, neutralized with glacial acid, and concentrated to a residue which was partitioned between methylene chloride and water. The organic extract was dried over anhydrous sodium sulfate and concentrated to give 2 (34 g, 97%). <sup>1</sup>H NMR (CDCl<sub>3</sub>): δ 1.50–4.70 (m, 9H), 7.29–8.01 (m, 5H), 10.89 (s, 1H). The latter was used without further purification.

**Procedure A: Compounds 3a–b. 1-Benzoyl-4-benzoylpiperidine (3a).** Oxalyl chloride (12.2 mL, 35.0 mmol) was added to a solution of compound 2 (7.92 g, 34.0 mmol) in methylene chloride, and the solution was stirred overnight at room temperature under

N<sub>2</sub>. Evaporation of solvent and other volatiles under reduced pressure provided the crude acyl chloride which was redissolved in dry benzene (25 mL). To this solution, AlCl<sub>3</sub> (6.8 g, 51.0 mmol) was added portionwise over 30 min under N<sub>2</sub>. The reaction mixture was then refluxed overnight, allowed to cool, and poured onto crushed ice with vigorous stirring. The resulting mixture was extracted with methylene chloride (3 × 100 mL). The organic layer was dried with anhydrous Na<sub>2</sub>SO<sub>4</sub> and then concentrated to yield the crude product. The crude product was purified by column chromatography on silica gel with 3:7 acetone/hexane as mobile phase to give 3a (6 g, 60%). <sup>1</sup>H NMR (CDCl<sub>3</sub>): δ 1.70–4.85 (m, 9H), 7.30–7.96 (m, 10H).

**1-Benzoyl-4-(4-bromobenzoyl)piperidine (3b).** Compound 3b was prepared from compound 2 as described in procedure A using bromobenzene in place of benzene (10.8 g, 85%). <sup>1</sup>H NMR (CDCl<sub>3</sub>): δ 1.50–4.20 (m, 8H), 4.40–4.90 (s, 1H), 7.20–7.48 (m, 7H), 7.50–7.84 (m, 2H).

**1-Benzoyl-4-(4-phthalimidobenzoyl)piperidine (4).** A mixture of 3b (16.0 g, 43.0 mmol), potassium phthalimide (9.0 g, 51.63 mmol), and copper(I) iodide (16.0 g, 51.63 mmol) in freshly distilled dimethylacetamide (100 mL) was refluxed under N<sub>2</sub> for 72 h. After cooling to room temperature, the reaction mixture was treated with 0.6 N HCl (50 mL). The resulting precipitate was removed by filtration. The filtrate was extracted with ethyl acetate (3 × 60 mL) and methylene chloride (3 × 100 mL). The combined organic solution was dried with anhydrous sodium sulfate and concentrated. The residue was purified on silica gel column with 40% ethyl acetate and 60% hexane as mobile phase to give 4 (18.0 g, 95%). <sup>1</sup>H NMR (CDCl<sub>3</sub>): δ 1.75–4.90 (m, 9H), 7.30–7.60 (s, 5H), 7.60–8.20 (m, 8H).

**1-Benzoyl-4-(4-aminobenzoyl)piperidine (3c).** A solution of 4 (0.7 g, 1.6 mmol) in 32% HBr–HOAc (60 mL) was stirred at 45 °C over 48 h until TLC demonstrated that the reaction was complete. The excess acid was removed by coevaporation with water (50 mL). The residue was treated with 30 mL of 0.1 N NaOH aqueous solution and then extracted consecutively with methylene chloride (3 × 30 mL) and ethyl acetate (2 × 30 mL). The combined organic solution was dried over anhydrous sodium sulfate and concentrated to generate 3c (0.45 g, 92%). <sup>1</sup>H NMR (CDCl<sub>3</sub>): δ 1.75–4.00 (m, 9H), 4.20–4.80 (d, 2H), 7.30–7.50 (s, 5H), 6.50–7.90 (d, 4H).

**1-Benzoyl-4-(4-nitrobenzoyl)piperidine (3d).** A solution of 3b (0.5 g, 1.62 mmol) in chloroform (20 mL) was added slowly to a refluxed solution of technical grade (55–75%) *m*-CPBA (5 g, 15.52 mmol) in chloroform (50 mL). The reaction mixture was refluxed until TLC demonstrated the reaction was complete. The reaction mixture was cooled to room temperature and treated with 10% NaHSO<sub>3</sub> (50 mL). The resulting mixture was washed with 0.2 N of NaOH aqueous solution. The organic layer was dried with anhydrous sodium sulfate and concentrated to a residue. The product was purified by radial flow chromatography with 15% of acetone and 85% of hexane as mobile phase to give 3d (0.33 g, 60%). <sup>1</sup>H NMR (CDCl<sub>3</sub>): δ 1.60–4.90 (m, 9H), 7.30–7.60 (m, 5H), 8.00–8.40 (d, 4H). EIMS calcd, 338.1267 (M<sup>+</sup>); found, 338.1275 (M<sup>+</sup>).

**Procedure B: Compounds 5a–d. 4-Benzoylpiperidine (5a).** A solution of compound 3a (5.6 g, 19.1 mmol) was refluxed in 6 N HCl (60 mL) overnight and monitored by TLC to demonstrate that the hydrolysis was complete. The reaction mixture was cooled to room temperature and extracted with methylene chloride (2 × 50 mL) to remove benzoic acid. The aqueous layer was concentrated to a residue which was treated with 0.1 N NaOH (50 mL). The resulting mixture was extracted with methylene chloride (3 × 60 mL) and ethyl acetate (2 × 50 mL). The combined organic extracts were dried over anhydrous sodium sulfate and concentrated to give 5a (3.2 g, 95%). <sup>1</sup>H NMR (CDCl<sub>3</sub>): δ 1.40–3.60 (m, 10H), 7.40–8.00 (m, 5H).

**4-(4-Bromobenzoyl)piperidine (5b).** Compound 5b was prepared from compound 3b as described in procedure B (4.8 g, 93%). <sup>1</sup>H NMR (CDCl<sub>3</sub>): δ 1.40–3.60 (m, 10H), 7.40–8.00 (m, 4H).

**4-(4-Aminobenzoyl)piperidine (5c).** Compound **5c** was prepared from compound **3c** as described in procedure B (3.0 g, 65%). <sup>1</sup>H NMR (DMSO-*d*<sub>6</sub> + CD<sub>3</sub>OD): δ 1.30–3.50 (m, 9H), 3.90–4.30 (s, 3H), 6.40–7.80 (d, 4H).

**4-(4-Nitrobenzoyl)piperidine (5d).** Compound **5d** was prepared from compound **3d** as described in procedure B (2.5 g, 70%). <sup>1</sup>H NMR (CDCl<sub>3</sub>): δ 1.60–1.80 (m, 4H), 1.90–2.00 (s, 1H), 2.70–2.85 (m, 2H), 3.10–3.25 (m, 2H), 3.25–3.40 (m, 1H), 8.06–8.10 (m, 2H), 8.30–8.40 (m, 2H).

**3-Bromo-1,2,3,4-tetrahydronaphthalen-2-ol (7).** 1,4-Dihydronaphthalene, **6** (5.12 g, 39.3 mmol), and *N*-bromosuccinimide (8.0 g, 44.9 mmol) were placed into 50 mL of 20% THF aqueous solution. The reaction mixture was stirred overnight and then extracted with methylene chloride (3 × 20 mL). The organic solution was combined and dried by anhydrous sodium sulfate. After concentration, the crude product was recrystallized from ethyl acetate and hexane to give **7** (8.0 g, 90%). <sup>1</sup>H NMR (CDCl<sub>3</sub>): δ 3.17 (s, 1H), 3.24 (s, 2H), 3.31 (s, 1H), 3.36–3.37 (d, 1H), 3.49 (s, 2H), 7.04–7.09 (m, 2H), 7.13–7.18 (m, 2H).

**1,2,3,4-Tetrahydronaphthalen-2,3-oxirane (8).** Compound **7** (2.16 g, 9.5 mmol) was dissolved in a 20 mL solution of 2.0 g of sodium hydroxide in 10 mL of water and 30 mL of chloroform. The reaction mixture was refluxed over 2 h until TLC indicated that the reaction was complete. The reaction mixture was extracted with methylene chloride (3 × 15 mL). The combined organic solution was dried by anhydrous sodium sulfate and concentrated. The crude product was purified on silica gel column with 10% of ethyl acetate and 90% of hexane mobile phase to give **8** (0.5 g, 35%). <sup>1</sup>H NMR (CDCl<sub>3</sub>): δ 3.17 (s, 1H), 3.24 (s, 2H), 3.31 (s, 1H), 3.36–3.37 (d, 1H), 3.49 (s, 2H), 7.04–7.09 (m, 2H), 7.13–7.18 (m, 2H).

**Procedure C: General Method for the Synthesis of Tetralins (9a–e).** (±)-*trans*-2-Hydroxy-3-(4-benzoylpiperidino)tetralin Hydrochloride (**9a**). To a solution of **8** (1.3 g, 8.8 mmol) in ethanol (50 mL), **5a** (155 g, 8.2 mmol) and sodium carbonate (4.0 g, 37.7 mmol) were added. The reaction mixture was refluxed over 42 h and then cooled to room temperature. The reaction mixture was filtered, and the precipitate was washed with a small amount of ethanol. The filtrate was concentrated to a residue. The residue was redissolved in methylene chloride (60 mL) and washed with brine. The organic solution was dried with anhydrous sodium sulfate and concentrated to a residue. The crude product was purified by radial flow chromatography to give **9a** (1.0 g, 35%). <sup>1</sup>H NMR (CDCl<sub>3</sub>): δ 1.60–3.30 (m, 14H), 3.30–3.40 (s, 1H), 3.80–4.00 (s, 1H), 6.90–7.30 (m, 4H), 7.40–8.10 (m, 5H). The hydrochloride was obtained from the methanolic hydrogen chloride solution and recrystallized from isopropyl alcohol/ethyl acetate, mp 242–243 °C. Anal. (C<sub>22</sub>H<sub>25</sub>NO<sub>2</sub>·HCl) C, H, N.

(±)-*trans*-2-Hydroxy-3-(4-(4-bromobenzoyl)piperidino)tetralin Hydrochloride (**9b**). Compound **9b** was prepared from compound **5b** as described in procedure C (2.4 g, 71%). <sup>1</sup>H NMR (CDCl<sub>3</sub>): δ 1.60–3.40 (m, 14H), 3.75–4.00 (s, 1H), 4.00–4.50 (s, 1H), 6.90–7.30 (m, 4H), 7.50–7.98 (d, 4H). The free base was converted to the hydrochloride by dissolving in methanolic HCl solution and recrystallized from isopropyl alcohol/diethyl ether, mp 271–273 °C. Anal. (C<sub>22</sub>H<sub>24</sub>BrNO<sub>2</sub>·HCl) C, H, N.

(±)-*trans*-2-Hydroxy-3-(4-(4-aminobenzoyl)piperidino)tetralin (**9c**). Compound **9c** was prepared from compound **5c** as described in procedure C (0.6 g, 48%), mp 70–73 °C. <sup>1</sup>H NMR (CDCl<sub>3</sub>): δ 1.70–3.80 (m, 8H), 3.80–4.00 (m, 1H), 4.00–4.70 (s, 3H), 6.90–7.60 (m, 4H), 6.50–8.40 (d, 4H). EIMS calcd, 350.1994 (M<sup>+</sup>); found, 350.1994 (M<sup>+</sup>).

(±)-*trans*-2-Hydroxy-3-(4-(4-nitrobenzoyl)piperidino)tetralin (**9d**). Compound **9d** was prepared from compound **5d** as described in procedure C (0.2 g, 48%). <sup>1</sup>H NMR (CDCl<sub>3</sub>): δ 1.50–3.70 (m, 8H), 3.70–4.00 (m, 1H), 4.00–4.70 (s, 1H), 6.90–7.50 (m, 4H), 7.90–8.45 (d, 4H). The purity of **9d** was greater than 95% (determined by HPLC).

**Resolution of Compound (±)-9d.** Chromatographic resolution of compound **9d** (0.230 g) was accomplished by HPLC using a 250 mm × 10 mm i.d. Chiralcel OD column (18:82 isopropanol/

hexane, 5.0 mL/min, UV wavelength 254 nm) to give 110 mg of (+)-**9d** (retention time, 22.3 min; enantiomeric purity, 99%) and 109 mg of (–)-**9d** (retention time, 38.13 min; enantiomeric purity, 99%). The specific rotation was determined on an automatic polarimeter (Autopol 111, Rudolph Research, Flanders, NJ). For the (+)-**9d**, the optical rotation [α]<sub>D</sub> is +37.0° with concentration as 5.68 mg/mL in methanol. For the (–)-**9c**, the optical rotation [α]<sub>D</sub> is –32.7° with concentration as 5.40 mg/mL in methanol.

(±)-*trans*-2-Hydroxy-3-(4-(4-fluorobenzoyl)piperidino)tetralin (**9e**). Compound **9e** was prepared from compound **5e** as described in procedure C (1.0 g, 61%). <sup>1</sup>H NMR [free base] (CDCl<sub>3</sub>): δ 1.60–2.10 (m, 4H), 2.42 (m, 1H), 2.70–3.60 (m, 8H), 3.88 (m, 1H), 6.90–7.30 (m, 6H), 7.97 (m, 2H). Anal. (C<sub>22</sub>H<sub>24</sub>FN<sub>2</sub>·HCl·0.25H<sub>2</sub>O) C, N, H.

**Resolution of Compound (±)-9e.** Chromatographic resolution of compound **9e** (0.170 g) was accomplished by HPLC using a 250 mm × 10 mm i.d. Chiralcel OD column (10:90 isopropanol/hexane, 5.0 mL/min, UV wavelength as 254 nm) to give 92 mg of (+)-**9e** (retention time, 14.9 min; enantiomeric purity, 99%) and 65 mg of (–)-**9e** (retention time, 25.2 min; enantiomeric purity, 99%). The optical rotation of (+)-**9e** is +40.6° with concentration of 5.4 mg/mL in methanol. The optical rotation of (–)-**9d** is –43.6° with concentration of 5.22 mg/mL in methanol. The purity of (+)-**9e** was 99% (determined by HPLC). The purity of (–)-**9e** was 99% (determined by HPLC).

**X-Ray Diffraction study of (–)-9e.** Crystals of appropriate dimension were obtained by slow evaporation of ethanol/dichloromethane solutions at 23 °C. A crystal with approximate dimensions of 0.05 × 0.12 × 0.37 mm<sup>3</sup> was mounted on glass fibers in a random orientation. Preliminary examination and data collection were performed using a Bruker Kappa Apex II charge coupled device (CCD) detector system single crystal X-ray diffractometer equipped with an Oxford Cryostream LT device. All data were collected using graphite monochromated Mo Kα radiation (λ = 0.710 73 Å) from a fine focus sealed tube X-ray source. Preliminary unit cell constants were determined with a set of 36 narrow frame scans. Intensity data set included combinations of ω and φ scan frames with scan width of 0.5° and counting time of 20 s/frame at a crystal to detector distance of 4.0 cm. The collected frames were integrated using an orientation matrix determined from the narrow frame scans. Apex II and SAINT software packages (Bruker Analytical X-Ray, Madison, WI, 2006) were used for data collection and data integration. Analysis of the integrated data did not show any decay. Final cell constants were determined by global refinement of xyz centroids of 1393 reflections from the complete data set. Collected data were corrected for systematic errors using SADABS (Blessing, R. H. *Acta Crystallogr.* **1995**, *A51*, 33–38) based on the Laue symmetry using equivalent reflections.

Crystal data and intensity data collection parameters are listed in Supporting Information (Table 4).

Structure solution and refinement were carried out using the SHELXTL-PLUS software package (Sheldrick, G. M., Bruker Analytical X-Ray Division, Madison, WI, 2006). The structure was solved by direct methods and refined successfully in the space group, *P*2<sub>1</sub>. Full matrix least-squares refinement was carried out by minimizing Σw(F<sub>o</sub><sup>2</sup> – F<sub>c</sub><sup>2</sup>)<sup>2</sup>. The non-hydrogen atoms were refined anisotropically to convergence. All hydrogen atoms were treated using appropriate riding model (AFIX m3). The final residual values and structure refinement parameters are available in Supporting Information (Table 4). Complete listings of positional and isotropic displacement coefficients for hydrogen atoms and anisotropic displacement coefficients for the non-hydrogen atoms are available in Supporting Information (Tables 5–9).

**Radiochemistry. Procedure D: General Method for Radio-labeling *trans*-2-Hydroxy-3-(4-(4-fluorobenzoyl)piperidino)tetralin with [ <sup>18</sup>F]Fluoride ([<sup>18</sup>F]**9e**).** (±)-*trans*-2-Hydroxy-3-(4-(4-[<sup>18</sup>F]fluorobenzoyl)piperidino)tetralin ((±)-[<sup>18</sup>F]**9e**). A sample of 100–150 mCi [<sup>18</sup>F]fluoride was added to a reaction vessel containing 1.0 mg of K<sub>2</sub>CO<sub>3</sub> and Kryptofix (5–6 mg), and the solution was evaporated under argon (block temperature of 110 °C). Acetonitrile (3 × 1.0 mL) was added and evaporated to ensure

complete removal of water. After all the water was removed, 1.5–2.0 mg of the corresponding nitrobenzoylbenzovesamicol, ( $\pm$ )-**9d**, was dissolved in DMSO (300  $\mu$ L). The precursor solution was transferred into the reaction vessel containing [<sup>18</sup>F]fluoride/Kryptofix and K<sub>2</sub>CO<sub>3</sub>. The reaction tube was capped and briefly mixed and then subjected to microwave irradiation for 40 s at medium power (60 W) until TLC scanner indicated a suitable incorporation yield. TLC mobile phase was 25:75 methanol/methylene chloride. The R<sub>f</sub> value of the product is approximately 0.90.

The reaction mixture was diluted with 3.0 mL of HPLC mobile phase and passed through a light alumina Neutral Sep-Pak cartridge. The crude product was then loaded onto a C-18 Econosil semi-preparative HPLC column with UV wavelength of 254 nm. The HPLC system used a 5 mL injection loop. With 23:77 THF/0.1 M formate buffer as eluent at 3.5 mL/min flow rate, the retention time of the product was 12.6 min. The retention time of the precursor was approximately 19.6 min. After evaporation of the HPLC solvent, the radiotracer was dissolved in 3–5 mL of saline and filtered using a 0.22  $\mu$ m sterile syringe filter.

Quality control of the product was performed on an analytical HPLC system that consisted of an Alltech Econosil reversed-phase C-18 column (250 mm  $\times$  4.6 mm) with a mobile phase of 37:63 acetonitrile/0.1 M ammonium formate buffer (pH 4.0–4.5). At a flow rate of 1.5 mL/min, the ( $\pm$ )-[<sup>18</sup>F]**9e** sample was co-injected with cold standard of **9e** and monitored with a variable-wavelength detector set at 254 nm with sodium iodide scintillation detector. The retention time of the product is 6.37 min. Under the same conditions, the retention time of the precursor is 9.10 min. The labeling yield was 50–60% (decay corrected). Both the radiochemical purity and chemical purity are also greater than 99%. The specific activity was >2000 Ci/mmol. The entire procedure took  $\sim$ 2 h.

(+)-*trans*-2-Hydroxy-3-(4-(4-[<sup>18</sup>F]fluorobenzoyl)piperidino)tetralin ((+)-[<sup>18</sup>F]**9e**). Compound (+)-[<sup>18</sup>F]**9e** was prepared from (+)-**9d** as described in procedure D. The solution of the corresponding precursor (+)-**9d** in DMSO was transferred into the reaction vessel containing predried [<sup>18</sup>F]fluoride/Kryptofix and K<sub>2</sub>CO<sub>3</sub>. The reaction vessel was capped and then irradiated for 40 s by microwave at medium power (60 W). After the reaction vessel was cooled, the purification was performed as described above on the same HPLC system. The labeling yield was 50–60% (decay-corrected). The radiochemical purity is greater than 99% radiochemical purity, and chemical purity is also greater than 99%. The specific activity was >2000 Ci/mmol. The entire procedure took  $\sim$ 2 h.

(-)-*trans*-2-Hydroxy-3-(4-(4-[<sup>18</sup>F]fluorobenzoyl)piperidino)tetralin ((-)-[<sup>18</sup>F]**9e**). Compound (-)-[<sup>18</sup>F]**9e** was prepared from (-)-**9d** as described in procedure D. The solution of the corresponding precursor (-)-**9d** in DMSO was transferred into the reaction vessel containing predried [<sup>18</sup>F]fluoride/Kryptofix and K<sub>2</sub>CO<sub>3</sub>. The reaction vessel was capped and then irradiated for 40 s by microwave at medium power (60 W). After the reaction vessel was cooled, the purification was performed as described above on the same HPLC system. The labeling yield was 50–60% (decay-corrected). The radiochemical purity is greater than 99%, and chemical purity is also greater than 99%. The specific activity was >2000 Ci/mmol. The entire procedure took  $\sim$ 2 h.

**In Vitro Biological Evaluation: Vesicular Acetylcholine Transporter Binding.** Dissociation constants of novel compounds were determined by competition against the binding of 5 nM [<sup>3</sup>H]vesamicol to postnuclear supernatant prepared from PC12 cells stably expressing human VACHT according to the methods utilized by Parsons and colleagues.<sup>47</sup> Compounds were assayed in increments of 10-fold from 0.1 to 10 000 nM. The surfaces of containers were precoated with Sigmacote (Sigma-Aldrich, MO). Samples containing 200  $\mu$ g of postnuclear supernatant in 200  $\mu$ L were incubated at 22  $^{\circ}$ C for 24 h in 0.02% sodium azide. A volume of 90  $\mu$ L was filtered in duplicate through GF/F glass fiber filters coated with polyethylenimine and washed. Filter-bound radioactivity was determined by liquid scintillation spectrometry. Averaged data were fit by regression with a rectangular hyperbola to estimate IC<sub>50</sub>. All compounds were independently assayed at least two times.

**In Vitro Biological Evaluation:  $\sigma$  Receptor Binding Assays.** The compounds were dissolved in DMF, DMSO, or ethanol and then diluted in 50 mM Tris-HCl buffer containing 150 mM NaCl and 100 mM EDTA at pH 7.4 prior to performing the  $\sigma_1$  and  $\sigma_2$  receptor binding assays. The procedures for isolating the membrane homogenates and performing the  $\sigma_1$  and  $\sigma_2$  receptor binding assays have been described in detail previously.<sup>59,60</sup>

Briefly, the  $\sigma_1$  receptor binding assays were conducted in 96-well plates using guinea pig brain membrane homogenates ( $\sim$ 300  $\mu$ g of protein) and  $\sim$ 5 nM [<sup>3</sup>H](+)-pentazocine (34.9 Ci/mmol, Perkin-Elmer, Boston, MA). The total incubation time was 90 min at room temperature. Nonspecific binding was determined from samples that contained 10  $\mu$ M cold haloperidol. After 90 min, the reaction was terminated by the addition of 150  $\mu$ L of ice-cold wash buffer (10 mM Tris-HCl, 150 mM NaCl, pH 7.4) using a 96-channel transfer pipet (Fisher Scientific, Pittsburgh, PA). The samples were harvested and filtered rapidly through a 96-well fiber glass filter plate (Millipore, Billerica, MA) that had been presoaked with 100  $\mu$ L of 50 mM Tris-HCl buffer at pH 8.0 for 1 h. Each filter was washed 3 times with 200  $\mu$ L of ice-cold wash buffer and the filter counted in a Wallac 1450 MicroBeta liquid scintillation counter (Perkin-Elmer, Boston, MA).

The  $\sigma_2$  receptor binding assays were conducted using rat liver membrane homogenates ( $\sim$ 300  $\mu$ g of protein) and  $\sim$ 5 nM [<sup>3</sup>H]DTG (58.1 Ci/mmol, Perkin-Elmer, Boston, MA) in the presence of 1  $\mu$ M (+)-pentazocine to block  $\sigma_1$  sites. The incubation time was 2 h at room temperature. Nonspecific binding was determined from samples that contained 10  $\mu$ M cold haloperidol. All other procedures were identical to those described for the  $\sigma_1$  receptor binding assay above.

Data from the competitive inhibition experiments were modeled using nonlinear regression analysis to determine the concentration that inhibits 50% of the specific binding of the radioligand (IC<sub>50</sub> value). Competitive curves were best fit to a one-site fit and gave pseudo-Hill coefficients of 0.6–1.0. K<sub>i</sub> values were calculated using the method of Cheng and Prusoff<sup>61</sup> and are presented as the mean  $\pm$  1 SEM. For these calculations, we used a K<sub>d</sub> value of 7.89 nM for [<sup>3</sup>H](+)-pentazocine and guinea pig brain and a K<sub>d</sub> value of 30.73 nM for [<sup>3</sup>H]DTG and rat liver.<sup>60</sup>

**In Vivo Biodistribution and ex Vivo Autoradiography Studies.** All animal experiments were conducted in compliance with the Guidelines for the Care and Use of Research Animals established by Washington University's Animal Studies Committee. For the biodistribution studies, 25–35  $\mu$ Ci of ( $\pm$ )-[<sup>18</sup>F]**9e**, (+)-[<sup>18</sup>F]**9e**, or (-)-[<sup>18</sup>F]**9e** in 100–150  $\mu$ L of saline was injected via the tail vein into mature male Sprague–Dawley rats (250–400 g) under 2–3% isoflurane/oxygen anesthesia. Groups of at least four rats were used for each time point. At 5 min, 30 min, 1 h, and 2 h p.i., the groups of rats were again anesthetized and euthanized. The whole brain was quickly removed and dissected into segments consisting of hippocampus, striatum, cortex, and cerebellum. The remainder of the brain was also collected in order to determine total brain uptake. At the same time, samples of blood, lung, liver, kidney, muscle, fat, heart, and bone were removed and counted in a Beckman Gamma 8000 well counter with a standard dilution of the injectate. Tissues were weighed, and the %ID/g was calculated. The striatum/organ ratios were calculated by dividing the %ID/g of the striatum by the %ID/g of the nontarget tissue.

For the ex vivo electronic autoradiography study, a mature male Sprague–Dawley rat was injected with  $\sim$ 500  $\mu$ Ci of (-)-[<sup>18</sup>F]**9e** via the tail vein under isoflurane/oxygen anesthesia, allowed to recover, and then euthanized after 1 h as described above. The brain was quickly removed and placed in a metal brain matrix with slots spaced at 1 mm intervals. The brain was then frozen in the matrix and sectioned into 1 mm coronal slices. Brain slices were carefully removed from the brain matrix razor blades, placed on a clear sheet, covered with film, and counted using the Packard InstantImager. The photographic image was obtained using a flatbed scanner.

**In Vivo MicroPET Brain Imaging Studies in Male Rhesus Monkeys.** Three independent PET studies were done on adult male rhesus monkeys (~9–11 kg) with a microPET Focus 220 scanner (Concorde/CTI/Siemens Microsystems, Knoxville, TN).

The animals were fasted for 12 h before PET study. The animals were initially anesthetized using an intramuscular injection with ketamine (10 mg/kg) and glycopyrulate (0.13 mg/kg) and then transported to the PET scanner suit. Upon arrival, the animal was intubated with an endotracheal tube and anesthesia was maintained at 0.75–2.0% isoflurane/oxygen throughout the PET scanning procedure. After intubation, a percutaneous venous catheter was placed for radiotracer injection. Core temperature was kept constant at 37 °C with a heated water blanket. In each microPET scanning session, the head was positioned supine in the adjustable head holder with the brain in the center of the field of view. A 10 min transmission scan was performed to check positioning; once confirmed, a 45 min transmission scan was obtained for attenuation correction. Subsequently, a 2 h dynamic emission scan was acquired after administration of 5–7 mCi of (–)-[<sup>18</sup>F]9e via the venous catheter.

**MicroPET Image Processing and Analysis.** Acquired list mode data were histogrammed into a 3D set of sinograms and binned to the following time frames: 3 × 1 min, 4 × 2 min, 3 × 3 min, and 20 × 5 min. Sinogram data were corrected for attenuation and scatter. Maximum a posteriori (MAP) reconstructions were done with 18 iterations and a  $\beta$  value of 0.004. A 1.5 mm Gaussian filter was applied to smooth each MAP reconstructed image. These images were then coregistered with MRI images to accurately identify the regions of interest with Amira software (Visage Imaging, Inc., Carlsbad, CA). The 3D regions of interest were manually drawn through all planes of coregistered MRI images for the caudate, putamen, and cerebellum (Figure 5). The regions of interest were then overlaid on all reconstructed PET images to obtain time–activity curves. Activity measures were standardized to body weight and dose of radioactivity injected to yield standardized uptake value (SUV) (Figure 6A).

**Acknowledgment.** This work was supported by a Washington University Alzheimer Disease Research pilot grant (Grant NIA P50 AG05681-21 and NIH Grant 1P30NS048056-01). The authors gratefully thank William H. Margenau and Robert Dennett for their excellent technical assistance. Mass spectrometry was provided by the Washington University Mass Spectrometry Resource, an NIH Research Resource (Grant P41RR0954). Optical rotation was determined in the laboratory of Dr. Douglas F. Covey in the Department of Molecular Biology and Pharmacology of Washington University. X ray crystallography was conducted by Dr. Nigam P. Rath of the Department of Chemistry and Biochemistry at the University of Missouri at St. Louis.

**Supporting Information Available:** Crystal structure data for (–)-9e (final residual values, structure refinement parameters, complete listings of positional and isotropic displacement coefficients for hydrogen atoms, anisotropic displacement coefficients for the non-hydrogen atoms) and analytical data of new compounds. This material is available free of charge via the Internet at <http://pubs.acs.org>.

## References

- Davies, P.; Wolozin, B. L. Recent advances in the neurochemistry of Alzheimer's disease. *J. Clin. Psychiatry* **1987**, *48*, 23–30.
- DeKosky, S. T.; Scheff, S. W. Synapse loss in frontal cortex biopsies in Alzheimer's disease: correlation with cognitive severity. *Ann. Neurol.* **1990**, *27*, 457–464.
- Masliah, E.; Ellisman, M.; Carragher, B.; Mallory, M.; Young, S.; et al. Three-dimensional analysis of the relationship between synaptic pathology and neuropil threads in Alzheimer disease. *J. Neuropathol. Exp. Neurol.* **1992**, *51*, 404–414.
- Masliah, E.; Mallory, M.; Hansen, L.; Alford, M.; DeTeresa, R.; et al. Localization of amyloid precursor protein in GAP43-immunoreactive aberrant sprouting neurites in Alzheimer's disease. *Brain Res.* **1992**, *574*, 312–316.
- Samuel, W.; Terry, R. D.; DeTeresa, R.; Butters, N.; Masliah, E. Clinical correlates of cortical and nucleus basalis pathology in Alzheimer dementia. *Arch. Neurol.* **1994**, *51*, 772–778.
- Scheff, S. W.; DeKosky, S. T.; Price, D. A. Quantitative assessment of cortical synaptic density in Alzheimer's disease. *Neurobiol. Aging* **1990**, *11*, 29–37.
- Terry, R. D.; Masliah, E.; Salmon, D. P.; Butters, N.; DeTeresa, R.; et al. Physical basis of cognitive alterations in Alzheimer's disease: synapse loss is the major correlate of cognitive impairment. *Ann. Neurol.* **1991**, *30*, 572–580.
- Fodale, V.; Mafrica, F.; Caminiti, V.; Grasso, G. The cholinergic system in Down's syndrome. *J. Intellect. Disabil.* **2006**, *10*, 261–274.
- Holtzman, D. M.; Santucci, D.; Kilbridge, J.; Chua-Couzens, J.; Fontana, D. J.; et al. Developmental abnormalities and age-related neurodegeneration in a mouse model of Down syndrome. *Proc. Natl. Acad. Sci. U.S.A.* **1996**, *93*, 13333–13338.
- Kish, S. J.; Distefano, L. M.; Dozic, S.; Robitaille, Y.; Rajput, A.; et al. [<sup>3</sup>H]Vesamicol binding in human brain cholinergic deficiency disorders. *Neurosci. Lett.* **1990**, *117*, 347–352.
- Kishnani, P. S.; Sullivan, J. A.; Walter, B. K.; Spiridigliozzi, G. A.; Doraiswamy, P. M.; et al. Cholinergic therapy for Down's syndrome. *Lancet* **1999**, *353*, 1064–1065.
- Bohnen, N. I.; Kaufer, D. I.; Hendrickson, R.; Ivanco, L. S.; Lopresti, B. J.; et al. Cognitive correlates of cortical cholinergic denervation in Parkinson's disease and parkinsonian dementia. *J. Neurol.* **2006**, *253*, 242–247.
- Bohnen, N. I.; Kaufer, D. I.; Ivanco, L. S.; Lopresti, B.; Koeppe, R. A.; et al. Cortical cholinergic function is more severely affected in parkinsonian dementia than in Alzheimer disease: an in vivo positron emission tomographic study. *Arch. Neurol.* **2003**, *60*, 1745–1748.
- Jann, M. W. Implications for atypical antipsychotics in the treatment of schizophrenia: neurocognition effects and a neuroprotective hypothesis. *Pharmacotherapy* **2004**, *24*, 1759–1783.
- Berman, J. A.; Talmage, D. A.; Role, L. W. Cholinergic circuits and signaling in the pathophysiology of schizophrenia. *Int. Rev. Neurobiol.* **2007**, *78*, 193–223.
- Breese, C. R.; Lee, M. J.; Adams, C. E.; Sullivan, B.; Logel, J.; et al. Abnormal regulation of high affinity nicotinic receptors in subjects with schizophrenia. *Neuropsychopharmacology* **2000**, *23*, 351–364.
- Court, J.; Spurdin, D.; Lloyd, S.; McKeith, I.; Ballard, C.; et al. Neuronal nicotinic receptors in dementia with Lewy bodies and schizophrenia: alpha-bungarotoxin and nicotine binding in the thalamus. *J. Neurochem.* **1999**, *73*, 1590–1597.
- Raedler, T. J.; Knable, M. B.; Jones, D. W.; Urbina, R. A.; Gorey, J. G.; et al. In vivo determination of muscarinic acetylcholine receptor availability in schizophrenia. *Am. J. Psychiatry* **2003**, *160*, 118–127.
- Holt, D. J.; Bachus, S. E.; Hyde, T. M.; Wittie, M.; Herman, M. M.; et al. Reduced density of cholinergic interneurons in the ventral striatum in schizophrenia: an in situ hybridization study. *Biol. Psychiatry* **2005**, *58*, 408–416.
- Holt, D. J.; Herman, M. M.; Hyde, T. M.; Kleinman, J. E.; Sinton, C. M.; et al. Evidence for a deficit in cholinergic interneurons in the striatum in schizophrenia. *Neuroscience* **1999**, *94*, 21–31.
- Dickey, C. A.; Petrucelli, L. Current strategies for the treatment of Alzheimer's disease and other tauopathies. *Expert Opin. Ther. Targets* **2006**, *10*, 665–676.
- Geldmacher, D. S. Alzheimer's disease: current pharmacotherapy in the context of patient and family needs. *J. Am. Geriatr. Soc.* **2003**, *51*, S289–295.
- Lleo, A.; Greenberg, S. M.; Growdon, J. H. Current pharmacotherapy for Alzheimer's disease. *Annu. Rev. Med.* **2006**, *57*, 513–533.
- Malouf, R.; Birks, J. Donepezil for vascular cognitive impairment. *Cochrane Database Syst. Rev.* **2004**, CD004395.
- Marlatt, M. W.; Webber, K. M.; Moreira, P. I.; Lee, H. G.; Casadesus, G.; et al. Therapeutic opportunities in Alzheimer disease: one for all or all for one. *Curr. Med. Chem.* **2005**, *12*, 1137–1147.
- Martinez, A.; Castro, A. Novel cholinesterase inhibitors as future effective drugs for the treatment of Alzheimer's disease. *Expert Opin. Invest. Drugs* **2006**, *15*, 1–12.
- Racchi, M.; Mazzucchelli, M.; Porrello, E.; Lanni, C.; Govoni, S. Acetylcholinesterase inhibitors: novel activities of old molecules. *Pharmacol. Res.* **2004**, *50*, 441–451.
- Roman, G. C. Rivastigmine for subcortical vascular dementia. *Expert Rev. Neurother.* **2005**, *5*, 309–313.
- Chez, M. G.; Aimonovitch, M.; Buchanan, T.; Mrazek, S.; Tremb, R. J. Treating autistic spectrum disorders in children: utility of the cholinesterase inhibitor rivastigmine tartrate. *J. Child Neurol.* **2004**, *19*, 165–169.
- Heller, J. H.; Spiridigliozzi, G. A.; Crissman, B. G.; Sullivan, J. A.; Eells, R. L.; et al. Safety and efficacy of rivastigmine in adolescents with Down syndrome: a preliminary 20-week, open-label study. *J. Child Adolesc. Psychopharmacol.* **2006**, *16*, 755–765.

- (31) Kondoh, T.; Amamoto, N.; Doi, T.; Hamada, H.; Ogawa, Y.; et al. Dramatic improvement in Down syndrome-associated cognitive impairment with donepezil. *Ann. Pharmacother.* **2005**, *39*, 563–566.
- (32) Arvidsson, U.; Riedl, M.; Elde, R.; Meister, B. Vesicular acetylcholine transporter (VAChT) protein: a novel and unique marker for cholinergic neurons in the central and peripheral nervous systems. *J. Comp. Neurol.* **1997**, *378*, 454–467.
- (33) Bravo, D. T.; Kolmakova, N. G.; Parsons, S. M. Choline is transported by vesicular acetylcholine transporter. *J. Neurochem.* **2004**, *91*, 766–768.
- (34) Usdin, T. B.; Eiden, L. E.; Bonner, T. I.; Erickson, J. D. Molecular biology of the vesicular ACh transporter. *Trends Neurosci.* **1995**, *18*, 218–224.
- (35) Erickson, J. D.; Varoqui, H.; Schafer, M. K.; Modi, W.; Diebler, M. F.; et al. Functional identification of a vesicular acetylcholine transporter and its expression from a “cholinergic” gene locus. *J. Biol. Chem.* **1994**, *269*, 21929–21932.
- (36) Kitamoto, T.; Wang, W.; Salvaterra, P. M. Structure and organization of the *Drosophila* cholinergic locus. *J. Biol. Chem.* **1998**, *273*, 2706–2713.
- (37) Naciff, J. M.; Misawa, H.; Dedman, J. R. Molecular characterization of the mouse vesicular acetylcholine transporter gene. *NeuroReport* **1997**, *8*, 3467–3473.
- (38) Roghani, A.; Feldman, J.; Kohan, S. A.; Shirzadi, A.; Gundersen, C. B.; et al. Molecular cloning of a putative vesicular transporter for acetylcholine. *Proc. Natl. Acad. Sci. U.S.A.* **1994**, *91*, 10620–10624.
- (39) Varoqui, H.; Diebler, M. F.; Meunier, F. M.; Rand, J. B.; Usdin, T. B.; et al. Cloning and expression of the vesamicol binding protein from the marine ray Torpedo. Homology with the putative vesicular acetylcholine transporter UNC-17 from *Caenorhabditis elegans*. *FEBS Lett.* **1994**, *342*, 97–102.
- (40) Prado, V. F.; Martins-Silva, C.; de Castro, B. M.; Lima, R. F.; Barros, D. M.; et al. Mice deficient for the vesicular acetylcholine transporter are myasthenic and have deficits in object and social recognition. *Neuron* **2006**, *51*, 601–612.
- (41) Siegal, D.; Erickson, J.; Varoqui, H.; Ang, L.; Kalasinsky, K. S.; et al. Brain vesicular acetylcholine transporter in human users of drugs of abuse. *Synapse* **2004**, *52*, 223–232.
- (42) Terry, A. V., Jr.; Mahadik, S. P. Time-dependent cognitive deficits associated with first and second generation antipsychotics: cholinergic dysregulation as a potential mechanism. *J. Pharmacol. Exp. Ther.* **2007**, *320*, 961–968.
- (43) Efange, S. M.; Mach, R. H.; Smith, C. R.; Khare, A. B.; Foulon, C.; et al. Vesamicol analogues as sigma ligands. Molecular determinants of selectivity at the vesamicol receptor. *Biochem. Pharmacol.* **1995**, *49*, 791–797.
- (44) Jung, Y. W.; Frey, K. A.; Mulholland, G. K.; del Rosario, R.; Sherman, P. S.; et al. Vesamicol receptor mapping of brain cholinergic neurons with radioiodine-labeled positional isomers of benzo-vesamicol. *J. Med. Chem.* **1996**, *39*, 3331–3342.
- (45) Kuhl, D. E.; Minoshima, S.; Fessler, J. A.; Frey, K. A.; Foster, N. L.; et al. In vivo mapping of cholinergic terminals in normal aging, Alzheimer’s disease, and Parkinson’s disease. *Ann. Neurol.* **1996**, *40*, 399–410.
- (46) Scheunemann, M.; Sorger, D.; Wenzel, B.; Heinitz, K.; Schliebs, R.; et al. Synthesis of novel 4- and 5-substituted benzyl ether derivatives of vesamicol and in vitro evaluation of their binding properties to the vesicular acetylcholine transporter site. *Bioorg. Med. Chem.* **2004**, *12*, 1459–1465.
- (47) Zea-Ponce, Y.; Mavel, S.; Assaad, T.; Kruse, S. E.; Parsons, S. M.; et al. Synthesis and in vitro evaluation of new benzo-vesamicol analogues as potential imaging probes for the vesicular acetylcholine transporter. *Bioorg. Med. Chem.* **2005**, *13*, 745–753.
- (48) Shiba, K.; Ogawa, K.; Ishiwata, K.; Yajima, K.; Mori, H. Synthesis and binding affinities of methylvesamicol analogs for the acetylcholine transporter and sigma receptor. *Bioorg. Med. Chem.* **2006**, *14*, 2620–2626.
- (49) Efange, S. M.; Mach, R. H.; Khare, A.; Michelson, R. H.; Nowak, P. A.; et al. *p*-[<sup>18</sup>F]fluorobenzyltrozamicol ([<sup>18</sup>F]FBT): molecular decomposition–reconstitution approach to vesamicol receptor radioligands for positron emission tomography. *Appl. Radiat. Isot.* **1994**, *45*, 465–472.
- (50) Gage, H. D.; Voytko, M. L.; Ehrenkauf, R. L.; Tobin, J. R.; Efange, S. M.; et al. Reproducibility of repeated measures of cholinergic terminal density using. *J. Nucl. Med.* **2000**, *41*, 2069–2076.
- (51) Mach, R. H.; Voytko, M. L.; Ehrenkauf, R. L.; Nader, M. A.; Tobin, J. R.; et al. Imaging of cholinergic terminals using the radiotracer [<sup>18</sup>F](+)-4-fluorobenzyltrozamicol: in vitro binding studies and positron emission tomography studies in nonhuman primates. *Synapse* **1997**, *25*, 368–380.
- (52) Voytko, M. L. Nonhuman primates as models for aging and Alzheimer’s disease. *Lab. Anim. Sci.* **1998**, *48*, 611–617.
- (53) Laforest, R.; Rowland, D. J.; Welch, M. J. MicroPET imaging of non-conventional isotopes. *IEEE Trans. Nucl. Sci.* **2002**, *49*, 2119–2126.
- (54) Beattie, B. J.; Finn, R. D.; Rowland, D. J.; Pentlow, K. S. Quantitative imaging of bromine-76 and yttrium-86 with PET: a method for the removal of spurious activity introduced by cascade  $\gamma$  rays. *Med. Phys.* **2003**, *30*, 2410–2423.
- (55) Bai, B.; Ruangma, A.; Laforest, R.; Tai, Y.-C.; Leahy, R. M. Positron range modeling for statistical PET image reconstruction. *IEEE Trans. Nucl. Sci.—MIC Proc.* **2003**, *4*, 2501–2505.
- (56) Gundlach, A. L.; Largent, B. L.; Snyder, S. H. Characterization of phencyclidine and sigma receptor-binding sites in brain. *NIDA Res. Monogr.* **1986**, *64*, 1–13.
- (57) Efange, S. M. In vivo imaging of the vesicular acetylcholine transporter and the vesicular monoamine transporter. *FASEB J.* **2000**, *14*, 2401–2413.
- (58) Frey, K. A.; Wieland, D. M.; Kilbourn, M. R. Imaging of monoaminergic and cholinergic vesicular transporters in the brain. *Adv. Pharmacol.* **1998**, *42*, 269–272.
- (59) Tu, Z.; Xu, J.; Jones, L. A.; Li, S.; Dumstörff, C.; et al. Fluorine-18-labeled benzamide analogues for imaging the sigma2 receptor status of solid tumors with positron emission tomography. *J. Med. Chem.* **2007**, *50*, 3194–3204.
- (60) Xu, J.; Tu, Z.; Jones, L. A.; Vangveravong, S.; Wheeler, K. T.; et al. [<sup>3</sup>H]N-[4-(3,4-Dihydro-6,7-dimethoxyisoquinolin-2(1H)-yl)butyl]-2-methoxy-5-methylbenzamide: a novel sigma-2 receptor probe. *Eur. J. Pharmacol.* **2005**, *525*, 8–17.
- (61) Cheng, Y.; Prusoff, W. H. Relationship between the inhibition constant ( $K_i$ ) and the concentration of inhibitor which causes 50% inhibition ( $IC_{50}$ ) of an enzymatic reaction. *Biochem. Pharmacol.* **1973**, *22*, 3099–3108.
- (62) Rogers, G. A.; Kornreich, W. D.; Hand, K.; Parsons, S. M. Kinetic and equilibrium characterization of vesamicol receptor–ligand complexes with picomolar dissociation constants. *Mol. Pharmacol.* **1993**, *44*, 633–641.